Hybrid Solar-Fossil Fuel Power Generation
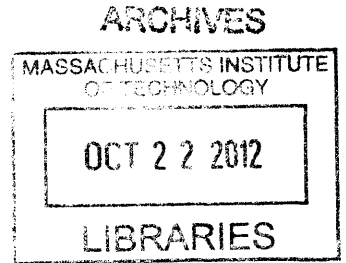
by

Elysia J. Sheu

Submitted to the Department of Mechanical Engineering
in partial fulfillment of the requirements for the degree of

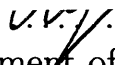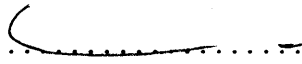Master of Science in Mechanical Engineering

at the

MASSACHUSETTS INSTITUTE OF TECHNOLOGY

September 2012

Author ....
Department of Mechanical Engineering
August 6, 2012

Certified by ....
Alexander Mitsos
Rockwell International Assistant Professor
Thesis Supervisor

Accepted by ....
David E. Hardt
Ralph E. and Eloise F. Cross Professor Of Mechanical Engineering
Chairman, Department Committee on Graduate Theses

Hybrid Solar-Fossil Fuel Power Generation

by

Elysia J. Sheu

Abstract

In this thesis, a literature review of hybrid solar-fossil fuel power generation is first given with an emphasis on system integration and evaluation. Hybrid systems are defined as those which use solar energy and fuel simultaneously, thus excluding the viable alternative of solar thermal plants which use fossil fuels as backup. The review is divided into three main sections: performance metrics, the different concentrated solar receiver technologies and their operating conditions, and the different hybridization schemes. In addition, a new linear combination metric for analysis of hybrid systems, which considers trade-off of different metrics at the fleet level, is presented. This metric is also compared to alternative metrics from multi-objective optimization. Some previous work only evaluates the hybrid cycle at a certain point in time, which can be misleading as this evaluation would not take into account certain aspects of hybrid cycle such as fluctuating solar supply. Furthermore, almost all previous work designs the hybrid solar-fossil fuel systems for a certain point in time and then evaluates the performance of the system for an entire year. By not taking into account fluctuating solar supply and selling price of electricity in the design of the system, the best possible annual performance of the hybrid cycle may not be reached.

Second, an analysis of solar reforming as the integration method for the hybrid cycle is presented, in particular steam reforming of methane. Two solar reforming systems are analyzed: one with a parabolic trough and the other with a solar tower. From the analysis, it is determined that parabolic troughs are not suitable for steam reforming due to the relatively low operating temperatures. The tower reformer system is integrated with a standard combined cycle, and the design and operation of the hybrid cycle is optimized for highest work output for a fixed fuel input and solar collector area (essentially optimizing for maximum cycle efficiency). A heuristic two step procedure is used for the optimization due to the limitation of the optimizer which cannot simultaneously optimize both design and operation. From the optimization, it is determined that the tower reforming integration method is a promising integration option in that this type of hybrid cycle yields high incremental solar efficiencies and also satisfies the linear combination metric for efficiency and CO_2 emissions (i.e., the analyzed hybrid cycle has a higher efficiency for a fixed CO_2 emissions compared to

a linear combination of solar only and fossil fuel only cycles).

Thesis Supervisor: Alexander Mitsos
Title: Rockwell International Assistant Professor

Acknowledgments

The work presented here in this thesis would not have been possible without the support of my family, friends, and colleagues. While it is impossible for me to thank everyone, I would like to thank a few people in particular.

First and foremost, I would like to thank my advisor for all the time and effort he has put into helping me with my work. Without his sacrifice, I would not have been able to fully enjoy my research experience.

Secondly, I want to thank my parents for all the support and inspiration they have given me and my brother for constantly being there whenever I need him. I want to also thank my cousins for giving me their support.

Thirdly, I want to thank my coauthors and colleagues for their insightful discussions which have benefited my work tremendously.

Contents

List of Figures

9

List of Tables

Chapter 1

A Review of Hybrid Solar-Fossil Fuel Power Generation Systems and Performance Metrics [105]

1.1 Introduction

As the world's population and economy continues to grow, electricity demand is expected to continue to increase, leading to higher CO_2 emissions. In order to reduce emissions, much research has been done investigating the use of renewable energy sources, such as solar energy, for power production. Solar energy, at least in principle, has the potential to provide all of the world's energy demands due to the large amount of insolation available from the sun; however, at the present time, only a small amount of the world's energy demand comes directly from solar energy. One reason for the lack of solar energy utilization is that even at optimal locations, large collecting areas are required which leads to higher costs as compared to other renewable/fossil technologies [118]. Another reason is that the solar supply is variable through the day which means that without some method of energy storage, power production from solar is intermittent and not dispatchable. On the other hand, storage leads to increased capital costs (even though the levelized cost can be lower with proper storage

[89, 12]). One potential solution to overcoming these intermittency and cost issues is hybrid concentrated solar-fossil fuel power generation. Other hybrid concepts such as solar with biomass fuel or solar with fossil fuel and wind are also promising, however, this review will focus on hybrid solar-fossil fuel. Hybrid solar-fossil fuel generation is defined here as a power cycle that whenever it utilizes solar energy, it also uses fuel. This somewhat arbitrary definition excludes, for instance, a solar thermal plant using fuel as backup when there is not enough solar insolation. Such concepts are a promising option for solar utilization, but are excluded herein because these solar thermal plants are already extensively reviewed in [13, 72, 120]. This review does discuss some comparison between these hybrid and solar thermal plants (in particular with the linear combination metric in Section 1.2), but a detailed comparison is outside the scope of this review.

In addition to reduced fuel consumption and emissions as compared to fossil fuel power generation [47, 116] and lower investment costs when compared to solar only power plants, hybrid power generation has the following two main advantages: 1) It is suitable for large-scale central electric power generation plants that can be integrated into the power grid because it does not have the grid connectivity problems (i.e., the need for synchronous reserve for frequency stabilization, fast power-ramping rates, differences between times of peak supply and demand, etc.) that arise with Concentrated Solar Power (CSP) or Photovoltaic (PV) plants without storage that are subjected to interruptions and variable solar supply [123] and 2) the solar application can be retrofitted to already-existing fossil fuel power plants (depending on site resources and power cycle design). With regards to the first advantage, solar only plants with proper storage or smart grid technology are also a promising option to eliminate grid connectivity problems traditionally associated with solar [99].

Currently used or studied hybrid power generation processes can be grouped into three main areas: solarized gas turbines, hybrid combined cycles, and solar reforming. This article discusses these three main hybridization schemes with emphasis on overall system design and integration, as opposed to, for example, solar reforming catalysts. First, the different metrics typically used to characterize and evaluate hybrid

14

solar-fossil fuel system performance are discussed and a new metric for comparison at the fleet level is proposed. Then, the different concentrated solar receiver technologies and their operating conditions are briefly discussed in order to illustrate how different solar technologies should be primarily used for integration within a hybrid cycle based on the temperatures required for the power generation. Finally, the three main hybridization schemes are discussed.

1.2 Performance and Design Metrics

Within previous literature, many different metrics are used to characterize and evaluate hybrid cycles. However, there is not a single source where all these metrics are presented and concisely explained and compared. In addition, some previous work use these metrics to evaluate the performance of a hybrid cycle at a certain point in time rather than over a time interval (which would take into account the fluctuation of solar supply, the time value of electricity, and give more representative results). Therefore, in addition to summarizing and explaining all previously used metrics, time integral metrics are also given. Also, a new linear combination metrics is proposed to allow for simultaneous evaluation of two metrics for a cycle.

The loss mechanisms associated with different solar technologies are first discussed followed by a discussion of the thermodynamic and economic metrics, the time interval metrics, and the new linear combination metric.

1.2.1 Solar Efficiency

Concentrated solar technologies are made up of two main components: the collectors and the receivers. For example, in a parabolic trough, these are the parabolic solar collectors and the receiver pipe. For each system there is an optical efficiency associated with the collector and then there is a system efficiency which depends on the optical efficiency as well as various loss mechanisms.

The main loss mechanisms for parabolic troughs and Fresnel reflectors (Section 1.3.1) include heat losses to the environment through convection and radiation. Also,

15

there are losses associated with the amount of radiation absorbed by the receiver pipe, cosine losses, and the reflectivity of the mirrors. There is also the loss due to the end effect, which is where, due to the tracking mode of the parabolic collector, the solar irradiation ends up being focused a bit beyond the length of the receiver tube. Spillage is a relative insignificant loss mechanism for parabolic troughs [57].

For the central receiver technologies (Section 1.3.2) loss mechanisms include heat losses due to convection and radiation (like parabolic troughs), however, they are significantly lower than the heat losses in a parabolic trough. There are also losses due to radiation spillage, shadowing of the collectors by the receiver, atmospheric attenuation, and blockage effects [46]. However, the main loss mechanism is due to the cosine efficiencies of the heliostats.

Finally, for solar-dish (Section 1.3.3), loss mechanisms are similar to other CSP technologies including heat losses and reflectivity losses [32].

All of these different loss mechanisms contribute to both the optical and system efficiencies.

1.2.2 Cycle Performance

For hybrid concentrated solar-fossil fuel cycles a number of metrics are used to evaluate cycle performance. These metrics can be grouped into first law efficiencies, second law efficiencies, solar-related metrics, and economic metrics. Most metrics can be either defined instantaneously or for a period of time (i.e., annualized). The metrics definitions discussed herein will be for a single point in time and then a discussion on how these metrics can be transformed into a metric for a period of time will be presented. In addition, a new linear combination metric will be presented. A summary of the different metrics previously used in literature is shown in Tab. 1.3 and Tab. 1.4.

Thermodynamic Metrics

First Law Efficiency

For a hybrid solar power cycle the first law system efficiency is defined as

$$\eta_I = \frac{\dot{W}}{\dot{Q}_{fuel} + \dot{Q}_{solar}}$$

where $\dot{W}$ is the net work output of the cycle, $\dot{Q}_{fuel}$ is the "heating rate" input from the fuel, and $\dot{Q}_{solar}$ is the energy rate input from the solar [16]. In the absence of fossil fuel, this efficiency is the so called solar to electric efficiency.

The heating rate is defined as $\dot{Q}_{fuel} = \dot{m}_{fuel} \cdot \text{LHV}$ where LHV is the lower heating value of the fuel (per unit mass) and $\dot{m}_{fuel}$ is the mass flow rate of the fuel used in the cycle. $\dot{Q}_{solar}$ is defined as $\dot{Q}_{solar} = \dot{q} \cdot A_a$ where $\dot{q}$ is the incident solar radiation and A_a is the collector area. The reason to include the total area of collector in the solar input calculation, e.g., as opposed to the solar heat reaching the cycle, is because this represents the total heating rate to the system accounting for optical losses. In addition, a substantial fraction of the capital cost is the collector area, which will only be taken into account if the total collector area is used in the solar input calculation.

The first law system efficiency has also been defined without the solar input as

$$\eta_{I,no-solar} = \frac{\dot{W}}{\dot{Q}_{fuel}}$$

However, this metric can be misleading since it is a monotonically increasing function of solar share which will be defined later. It essentially considers the solar energy to be "free" which is unrealistic. Moreover, this metric is very similar to the CO_2 emissions metric (merely take the inverse of the fuel only efficiency and multiply by the emissions of the fuel to get the CO_2 emissions), and therefore does not give any new insight.

Second Law efficiency

The second law system efficiency for a hybrid solar power cycle is defined as

$$\eta_{II} = \frac{\dot{W}}{\dot{E}_{fuel} + \dot{E}_{solar}}$$

17

where $\dot{E}_{fuel}$ is the exergy rate of the fuel and $\dot{E}_{solar}$ is the exergy rate of solar input [16].

There are numerous ways of calculating solar exergy. One class of methods is to consider a "thermodynamic system" where a certain volume is initially filled with equilibrium blackbody radiation. The exergy of this system is then determined by how much work can be extracted from this system as it reaches the "dead" state. One common approach, within this first class, to calculating the exergy of the solar input is as follows [55, 122]

$$\dot{E}_{solar} = \dot{Q}_{solar} \left(1 - \frac{T_o}{T_i} \right)$$

where T_o is the ambient temperature and T_i is the temperature of the solar source (temperature of sun surface $\approx$ 5800K). Another similar method is suggested by Spanner as follows[109]

$$\dot{E}_{solar} = \dot{Q}_{solar} \left(1 - \frac{4T_o}{3T_i} \right)$$

This method of calculation is similar to the first method discussed, however, 3/4 of the temperature of the sun surface is used (hence the factor of 4/3 in front of the temperature ratio). A third method, within this first class of exergy calculation methods, is suggested by Petela and is based on a quartic function for temperature [86, 87]:

$$\dot{E}_{solar} = \dot{Q}_{solar} \left(1 + \frac{1}{3} \left(\frac{T_o}{T_i} \right)^4 - \frac{4T_o}{3T_i} \right)$$

This quartic equation is based on the exergy of isotropic blackbody radiation for a deformable reflecting enclosure and better represents the radiation that actually reaches the earth's surface.

While these three methods of calculation may seem very different and contradicting, Bejan argues that these three theories are in fact complementary. The differences in each approach are due to the difference in understanding of how to describe the "investment" made by thermal radiation in the production of work and how to appropriately model the radiation system [19]. It is also important to note that for all

three estimations of the solar exergy, the exergy transfer rate is approximately equal to the heat transfer rate ($\dot{E}_{solar} \approx x\dot{Q}_{solar}$ where x is between 93% and 95%).

The second class of exergy calculation methods is to consider the emission of solar radiation into the environment and determine how much mechanical power can be produced with the portion of solar emission that can be intercepted by a collector [19]. There are many models to approximate the collector which can be found in [20]. One model is to assume that the collector is in thermal contact only with the sun. In that case, for a given heat transfer rate $\dot{Q}$ the maximum power is given by $\dot{Q}(1 - \frac{T_o}{T_i})$ which can be used as the exergy. However, the maximum power requires the collector temperature T_c to be equal to the sun temperature, implying zero heat transfer per unit area. It is thus sensible to calculate the efficiency as $\frac{\dot{W}}{\sigma AT_i^4} = \left(1 - \left(\frac{T_cT_i}{T_o^2}\right)^4 \left(1 - \frac{T_o}{T_c}\right)\right)$. For standard ambient conditions the maximum of this expression is ≈ 0.85 [20]. More complicated models account also for heat losses to the ambient.

Recently Zamfirescu and Dincer [126] presented a method, wherein the solar exergy is also dependent on the solar constant, the solar insolation, and incidence angle. This method gives lower values of exergy than most other methods discussed previously with exergy values being as low as 85% of the energy value for times near sunset and sunrise. However, the lower fraction still does not give significantly different values for solar exergy and energy for the majority of the day.

The exergy of the fuel can be calculated based on the combustion reaction as follows

$$\xi^o_{fuel} = -\Delta_R G^{oo} + T_o \ln \left(\prod_{i \neq fuel} \frac{R}{MM_i} \left(x_i \frac{MM_{tot}}{MM_i} \right)^{-\nu_i} \right)$$

where ξ^o_{fuel} is the standard mass exergy of the fuel, $\Delta_R G^{oo}$ is the Gibbs Free Energy of reaction at standard pressure and temperature, R is the universal gas constant, T_o is the ambient temperature, x_i is the mass fraction of species i in the environment, MM_{tot} is the molar mass of all the species i combined, MM_i is the molar mass of species i in the environment, and ν_i is the stoichiometric coefficient of species i (species i refers to all species in the combustion reaction except for the fuel) [21]. For this calculation,

water is considered to be in the vapor phase, which is consistent with the use of the LHV.

The second law efficiency is in principle, a better measure of hybrid cycle efficiency than the first law efficiency because it takes into account weighted contributions of the two input sources. However, as seen in Tab. 1.1, for most fuels of interest, the exergy of the fuel is approximately equal to the LHV. Therefore, since the solar exergy is also approximately equal to the solar energy (as discussed before), the second law efficiency is approximately equal to the first law efficiency for any hybrid system.

Table 1.1: Exergy values, LHVs, and f_{CO_2} values of fuels most commonly used in hybrid cycles (assumed composition of fuel in parentheses)[39, 68, 97]

Fuel	Exergy Value (MJ/kg)	LHV (MJ/kg)	f_{CO_2} (kg CO_2/MJ)
Natural Gas (CH_4)	52	50	0.055
Coal (C)	26	23	0.159
Oil (C_8H_{18})	45.5	43	0.072

Solar-Related Metrics

For almost all solar-related metrics, a "reference" plant is used as part of the metric. The "reference" plant is typically taken to be the highest efficiency plant with the same flowsheet as the hybrid plant except there is no solar application. The fuel type and fuel flow rate are the same for both, but the operating conditions are not necessarily the same [100]. However, a better reference plant would be the highest efficiency plant in general (i.e., for a hybrid combined cycle, the reference plant would be a standard highest efficiency combined cycle rather than one that is exactly the same as the hybrid plant) because this allows for comparison with traditional plants in a more generalized sense rather than a specific case. In either case, the efficiency of the reference plant is given by

$$\eta_{ref} = \frac{\dot{W}_{ref}}{\dot{Q}_{fuel,hybrid}}$$

20

where $\dot{W}_{ref}$ is the work output of the reference plant given the same input of fuel as the hybrid plant.

A metric commonly used to characterize hybrid cycles is the solar share. The solar share can be defined in two different ways: either based on the energy input or the work output. The solar share based on the energy input is defined as [57]

$$X_{s,i} = \frac{\dot{Q}_{solar}}{\dot{Q}_{fuel} + \dot{Q}_{solar}}$$

For the work output basis, the solar share is defined as [100]

$$X_{s,o} = \frac{\dot{W} - \eta_{ref}\dot{m}_{fuel}LHV}{\dot{W}}$$

where $\dot{m}_{fuel}$ is the amount of fuel consumed by the hybrid cycle, η_{ref} is the efficiency of the reference plant, and $\dot{W}$ refers to the work output of the hybrid cycle.

Solar share may have an upper limit significantly less than one due to the fact that the power cycle will most likely run even when there is no solar. Also, note that the output and input solar share are not the same unless the efficiencies of the hybrid and reference plant are equal.

Another measure of performance of a hybrid cycle besides the cycle efficiency is the net incremental solar efficiency which is defined as

$$\eta_{net-incr-solar} = \frac{\dot{W} - \eta_{ref}\dot{m}_{fuel}LHV}{\dot{Q}_{solar}}$$

where $\dot{m}$ is the flow rate of the fuel, and η_{ref} is the overall net electric efficiency of the "reference" plant [34].

This incremental solar efficiency can be negative for, e.g., insignificant output solar shares, so therefore, this metric can be used to determine a bad integration method. An example would be if the solar application was integrated in a gas turbine such that the solar energy is used to heat the flue gases after combustion. In this case, since the flue gases are already at high temperatures, which the solar application cannot necessarily reach, the amount of heating supplied by the solar application would

be minimal, regardless of input solar share, unless the combustion temperature is lowered. Therefore, with the lower combustion temperature, the overall efficiency of the hybrid plant would decrease and no "extra" power would be produced leading to a negative incremental solar efficiency. Therefore, the net incremental solar efficiency would be negative since the work output from the hybrid plant would be less than the reference plant.

Another design parameter traditionally used for solar applications is the solar multiple. The solar multiple is defined as

$$\text{SM} = \frac{\dot{Q}_{solar}}{\dot{Q}_{power-block}}$$

where $\dot{Q}_{solar}$ is the thermal power produced by the solar field at the design point and $\dot{Q}_{power-block}$ is the thermal power (from solar) required by the power cycle at nominal conditions [77]. The above definition is used for solar only plants, however, when applied to a hybrid cycle, the solar multiple is not independent of the input solar share, and therefore not a design metric likely to be used for hybrid cycles.

One other performance metric is the incremental CO_2 avoidance which is defined as

$$\Delta CO_2 = \left(\frac{\dot{W}}{\eta_{ref}} - \dot{Q}_{fuel} \right) \cdot f_{CO_2}$$

where f_{CO_2} is the amount of CO_2 emissions per heating rate of fuel [100]. Values of f_{CO_2} for a few common fuels are given in Tab. 1.1. Similar to the incremental solar efficiency, this metric can also be negative for poor designs.

In addition to these different solar-related metrics, the ecological footprint of the solar application should also be taken into account. More specifically, the land area needed for the solar field should be considered as this will not only affect the cost of the solar application but also the use of this land for the solar field can compete with other important land uses such as agriculture or wildlife. Concentrated solar, like most renewable energy technologies, has low energy density and thus requires large land areas, usually on the order of $15768 - 22776$ m^2/MW [90]. However, one

22

advantage for solar in terms of land usage is that solar fields can be placed on hillsides [42, 78, 107, 108] or in desserts, i.e., utilize land that is otherwise not very valuable. Moreover, a recent proposal for a biomimetic heliostat layout greatly reduces land area of central receiver solar plants while simultaneously increasing field efficiency for power generation [79].

Economic Metrics

The most common evaluation parameter of economic performance is levelized electricity cost (LEC), which is expressed as

$$\text{LEC} = \frac{I_{PV}^{ann} + \text{OM}_{PV}^{ann} + F_{PV}^{ann}}{E_{gen}^{ann}}$$

where I_{PV}^{ann} is the annualized present value of total investment cost, OM_{PV}^{ann} is the annualized present value of the operating and maintenance cost, F_{PV}^{ann} is the present value of the annual fixed cost, and E_{gen}^{ann} is the annual electricity output [34].

The solar LEC (SLEC) is the LEC of the electricity produced from the solar application. The solar LEC can be calculated as

$$\text{SLEC} = \frac{\text{LEC} - [(1 - X_{s,o}) \cdot \text{LEC}_{ref}]}{X_{s,o}}$$

This SLEC approximates the LEC of the electricity that is produced by only the solar part of the hybrid plant. The second term of the numerator represents the LEC of the electricity produced by the fuel in the hybrid plant, and the difference between the total LEC and the LEC of the fuel portion is divided by the solar share to represent the LEC of the portion of electricity produced by the hybrid plant from the solar part [34, 54].

Herein, a different definition for SLEC is given as

$$\overline{\text{SLEC}} = \frac{(I_{PV}^{ann} + \text{OM}_{PV}^{ann} + F_{PV}^{ann})_{solar}}{X_{s,o} E_{gen}^{ann}}$$

This calculation of SLEC is different from the one presented in [34, 54] since the

23

output solar share does not necessarily represent the portion of total cost associated with the solar. To illustrate that the two definitions are different, consider a fictitious scenario with the parameters shown in Tab. 1.2. Based on the parameters in Tab. 1.2 the SLEC is \$0.38/kWh, while the $\overline{\text{SLEC}}$ is \$0.33/kWh.

Table 1.2: Fictitious SLEC Example

Parameter	Value
$(I_{PV}^{ann} + OM_{PV}^{ann} + F_{PV}^{ann})_{solar}$	\$ 9.75 million
$(I_{PV}^{ann} + OM_{PV}^{ann} + F_{PV}^{ann})_{fossilfuel}$	\$ 5.25 million
Total Electricity Produced	100 GWh
Output Solar Share	30%
Reference Plant LEC	\$ 0.05/kWh
LEC	\$ 0.15/kWh
SLEC	\$ 0.38/kWh
$\overline{\text{SLEC}}$	\$ 0.33/kWh

In this fictitious example, the SLEC is higher than the $\overline{\text{SLEC}}$ because the SLEC determines the cost of the electricity produced from the fuel input of the hybrid cycle using the LEC of the reference plant; however, since the hybrid cycle and the reference plant are most likely operating at different conditions, the LEC of the fuel input in the hybrid cycle is most likely higher than the LEC of the reference plant. In other words, the LEC of the hybrid cycle with an input solar share of zero would most likely be higher than the LEC of the reference plant. Therefore, since the LEC of the reference plant used in this example is most likely lower than the fuel LEC of the hybrid plant, the SLEC is higher.

Essentially the main difference between the SLEC and the $\overline{\text{SLEC}}$ is that the $\overline{\text{SLEC}}$ is independent of the reference plant, which can be somewhat arbitrary in its definition making it difficult to determine the true LEC of the hybrid cycle fuel input. However, it is also difficult to determine solar portion of the total cost of the hybrid plant. Therefore, these two definitions differ in how the division of solar and fuel cost is determined. It should also be noted that these two definitions would be the same if

the total cost of the reference plant is the same as the cost of the fossil fuel part of the hybrid cycle. However, this would most likely not be the case as, for example, if the solar is integrated into the steam cycle, the steam turbines would need to be larger to accommodate the increase in steam flow rate, which would mean that the cost of the fossil fuel portion of the hybrid cycle (the power cycle) would be higher than the total cost of the reference plant (which would have smaller turbines).

Time Interval Metrics

Most metrics used in literature are for a certain point in time, however, a more representative metric for evaluation would be one that is for a certain time interval (in particular annual) because this would account for the fluctuation of solar. These time interval metrics can be derived from the instantaneous definitions via an average or weighted integral to take into account fluctuating solar supply, fuel price, and electricity demand. The annual first law efficiency is shown below [100].

$$\eta_I = \frac{W}{Q_{fuel} + A_a \cdot \int_{ann} \text{DNI}(t)\,dt}$$

where W and Q_{fuel} is the total work output and fuel input for the entire year, respectively, and DNI is the direct normal irradiance as a function of time for the entire year. Other annualized metrics are shown in Tab. 1.3 and Tab. 1.4.

The LEC is by definition annualized, but a better representation for cost may be a LEC that takes into account time variations. In general, LEC is calculated by dividing total cost of the plant by the amount of electrical energy produced by the plant. However, the capital, operating, and maintenance costs are time-dependent (in that present day value is used). Therefore, a time variable LEC would take into account how valuable power is depending on demand, and therefore, this "worth" should be factored into the calculation of the LEC through some weighted function for the power produced that is dependent on time. There are also proposals for time dependent feed-in tariff since these lead to more rational operation [41, 43]. Alternatively, the LEC could also give some value to dispatchability (e.g., when energy is stored instead of

25

used immediately). Under rational energy policies, or in a free market with time-variable electricity price, a plant with high LEC but dispatchable power can be more profitable than plants with low LEC that cannot produce dispatchable power [94].

Table 1.3: Summary of performance metrics used in literature [16, 34, 100]

Metric	Instantaneous Definition	Annual Definition
First Law System Efficiency	$\eta_I = \dfrac{\dot{W}}{Q_{fuel}+Q_{solar}}$	$\eta_I = \dfrac{W}{Q_{fuel}+A_a \cdot \int_{ann} DNI(t)\,dt}$
First Law System Efficiency (no solar)	$\eta_{I,no-solar} = \dfrac{\dot{W}}{Q_{fuel}}$	$\eta_{I,no-solar} = \dfrac{W}{Q_{fuel}}$
Second Law System Efficiency	$\eta_{II} = \dfrac{\dot{W}}{\dot{E}_{fuel}+\dot{E}_{solar}}$	$\eta_{II} = \dfrac{W}{E_{fuel}+E_{solar}}$
Incremental Solar Efficiency	$\eta_{net-incr-solar} = \dfrac{\dot{W}-\eta_{ref}\dot{Q}_{fuel}}{Q_{solar}}$	$\eta_{net-incr-solar} = \dfrac{W-\eta_{ref}Q_{fuel}}{A_a \cdot \int_{ann} DNI(t)\,dt}$
Incremental CO_2 Avoidance	$\Delta CO_2 = \left(\dfrac{\dot{W}}{\eta_{ref}} - \dot{Q}_{fuel}\right) \cdot f_{CO_2}$	$\Delta CO_2 = \left(\dfrac{W}{\eta_{ref}} - Q_{fuel}\right) \cdot f_{CO_2}$
Levelized Electricity Cost	-	$LEC = \dfrac{I_{PV}^{ann}+OM_{PV}^{ann}+F_{PV}^{ann}}{E_{gen}^{ann}}$
Solar Levelized Electricity Cost	-	$SLEC = \dfrac{LEC-[(1-X_{s,o}) \cdot LEC_{ref}]}{X_{s,o}}$

Linear Combination Metric

The metrics presented so far, such as incremental solar efficiency and LEC, are not enough to fully evaluate the performance of these hybrid cycles because they only consider a single aspect. A better metric may be one based on linear combinations of alternative technologies. This linear combination metric is based on the one presented in [71] for partial emission cycles. Essentially to determine the true potential of a hybrid cycle one needs to determine the best combination of all potential types of plants (fossil fuel, solar, or hybrid) for cost, emissions, and efficiency.

Let $\tau_{i,j}$ denote the performance of technology $i \in I$, measured by the metric $j \in J$.

Table 1.4: Summary of design metrics used in literature [16, 34, 77, 100]

Metric	Instantaneous Definition	Annual Definition
Solar Share (input)	$X_{s,i} = \dfrac{\dot{Q}_{solar}}{Q_{fuel}+Q_{solar}}$	$X_{s,i} = \dfrac{A_a \cdot \int_{ann}\mathrm{DNI}(t)\,dt}{Q_{fuel}+A_a \cdot \int_{ann}\mathrm{DNI}(t)\,dt}$
Solar Share (output)	$X_{s,o} = \dfrac{\dot{W}-\eta_{ref}\dot{Q}_{fuel}}{\dot{W}}$	$X_{s,o} = \dfrac{W-\eta_{ref}Q_{fuel}}{W}$
Solar Multiple	$\mathrm{SM} = \dfrac{\dot{Q}_{solar}}{\dot{Q}_{power-block}}$	$\mathrm{SM} = \dfrac{A_a \cdot \int_{ann}\mathrm{DNI}(t)\,dt}{Q_{power-block}}$

For simplicity, assume that the objective is to minimize all metrics (as opposed to maximizing some). Typically, there are tradeoffs between different metrics, and not all objectives can be simultaneously minimized. One way to deal with this tradeoff is to assign weights to the different metrics and optimize for the weighted objective. However, this is not desirable because it does not capture the tradeoffs, and the optimal answer depends on the weights chosen. Instead, in multi-objective optimization the notion of nondominated solutions or Pareto-optimal solutions is typically used, e.g., [85]. If there are many competing technologies, a candidate technology n is Pareto-optimal if and only if there exists no $i \in I$ such that

$$\forall j \in J : \tau_{i,j} \leq \tau_{n,j} \quad \text{and} \quad \exists j \in J : \tau_{i,j} < \tau_{n,j}.$$

In other words, to improve one of the metrics compared to technology n, another metric will be deteriorated. There are techniques to calculate the set of Pareto optimal solutions [66]. Pareto-optimization has been explored for power plants, e.g., in [67, 111, 38]. However, Pareto-optimality does not necessarily imply improvement over a linear combination of alternative technologies. Herein, it is proposed to only choose a technology if it improves one of the objectives compared to any possible linear combination (more precisely convex combination), of alternative technologies, which mathematically is expressed as: there exists no finite set $\hat{I} \subset I$ and $\lambda_i \in [0,1]$ with

27

$\sum_{i \in \hat{I}} \lambda_i = 1$, s.t.:

$$\forall j \in J : \sum_{i \in \hat{I}} \lambda_i \tau_{i,j} \leq \tau_{n,j} \quad \text{and} \quad \exists j \in J : \sum_{i \in \hat{I}} \lambda_i \tau_{i,j} < \tau_{n,j}.$$

The notion proposed is stronger than Pareto-optimal: a technology that satisfies the above criterion automatically is also a Pareto optimal solution, but not vice-versa. Another interpretation of the proposed metric is that it compares a given technology with the convex hull of the Pareto front. As an example, consider that two objectives are to be minimized, namely CO_2 emissions per power produced, and LEC. A hybrid plant must compete with fossil-fuel only plants and solar-only plants. Typically, fossil fuel plants have significantly lower LEC and higher emissions than renewables, and hybrid plants have intermediate values for both metrics

$$\text{LEC}_{fossil} \quad < \quad \text{LEC}_{hybrid} < \text{LEC}_{solar}$$

$$\text{CO}_{2,solar} \quad < \quad \text{CO}_{2,hybrid} < \text{CO}_{2,fossil}.$$

The hybrid cycle is a Pareto-optimal (nondominated) solution, since it can be seen as an improvement over fossil fuel plant in terms of emissions, or as an improvement over solar cycles in terms of LEC. However, the hybrid cycle needs to be compared also to combinations of solar only and fossil only plants, and it is only viable if for the same average LEC it has lower CO_2 emissions

$$\text{CO}_{2,hybrid} < \text{CO}_{2,fossil} + \frac{\text{LEC}_{hybrid} - \text{LEC}_{fossil}}{\text{LEC}_{solar} - \text{LEC}_{fossil}}(\text{CO}_{2,solar} - \text{CO}_{2,fossil})$$

or equivalently, if for the same average CO_2 emissions it has lower LEC

$$\text{LEC}_{hybrid} < \text{LEC}_{fossil} + \frac{\text{CO}_{2,hybrid} - \text{CO}_{2,fossil}}{\text{CO}_{2,solar} - \text{CO}_{2,fossil}}(\text{LEC}_{solar} - \text{LEC}_{fossil})$$

In other words, a hybrid cycle should improve on the two competing metrics at the fleet level.

Assume that the solar only, fossil fuel only, and hybrid plants have the parameters shown in Fig. 1-1 and each plant has a work output of 100 MW. Consequently, the proposed metric determines that the proposed hybrid cycle A is not competitive

because if one has to provide 1 GW of power, instead of building ten hybrid solar-fossil fuel A plants, one could build five solar only plants and five fossil fuel only plants which would have the same amount of emissions with a lower average LEC (0.13 $/kWh). Alternatively, one could build 6 solar only and 4 fossil fuel only plants, and this combination would achieve approximately the same average LEC and less overall emissions than 10 hybrid plants of technology A. In contrast, for hybrid cycle B, the linear combination metric shows that this hybrid cycle is a viable one because it gives a lower average LEC than a linear combination of the solar and fossil fuel only plants with the same CO_2 emissions or a lower CO_2 emissions for the same average LEC. Note that similar to Pareto optimization, the proposed metric generates a set of viable technologies, as opposed to a single optimal technology.
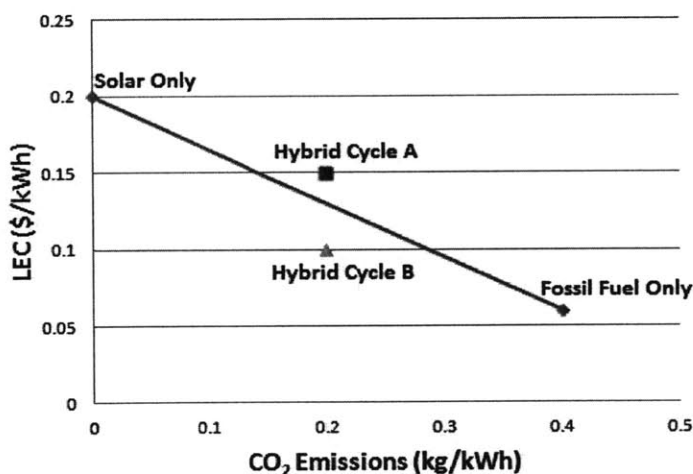
Figure 1-1: Fictitious example for linear combination metric: Assumed parameters of solar only, fossil fuel only, and hybrid plants (Hybrid Cycle B is competitive while Hybrid Cycle A is not)

To demonstrate that the proposed metric is an extension of the notion of Pareto-optimal solutions in multi-objective optimization, consider a fictitious scenario shown in Fig. 1-2. Therein, Hybrid Plant C is on the Pareto-optimal front, however, Hybrid Plant C should not be considered since a linear combination of solar only and fossil fuel only plants will have the same emissions with a lower average LEC or the same average LEC with lower emissions than Plant C. In other words, plant C is not dominated

29

by any single plant, but it is dominated by combinations and the proposed metric compares the performance of a given plant at the fleet level. Rather than merely optimizing a metric for a given plant, the most sensible use of resources is to consider the cumulative effect of all plants in operation or planned.
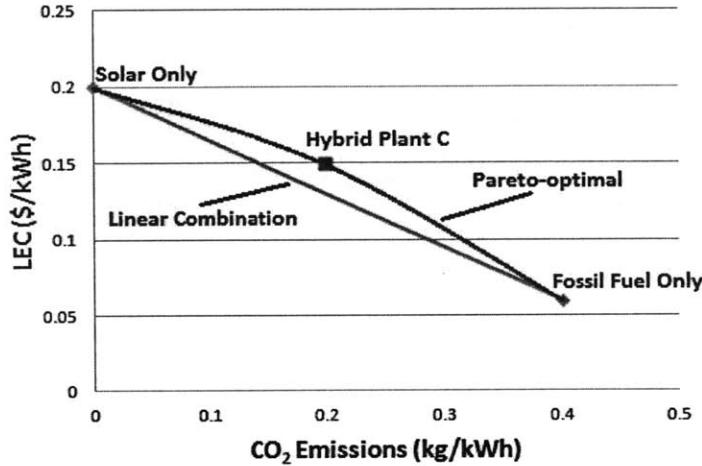
Figure 1-2: Fictitious scenario for comparison of Pareto-optimal and linear combination metric (Pareto-optimal points are not necessarily optimal under the metric proposed)

1.3 Concentrated Solar Receiver Technologies

In this section, the concentrated solar receiver technologies and their operating conditions will be discussed. A summary of the different technologies is shown in Tab. 1.5.

1.3.1 Parabolic Trough/Fresnel Reflectors

The parabolic trough technology is the most mature of the concentrated solar power technologies. It uses a single-axis tracking curved mirror system to concentrate solar radiation onto a receiver pipe which contains a heat transfer fluid. In most cases, the heat transfer fluid used is either a mineral oil or a synthetic thermal oil. This fluid is then most often used in a heat exchanger for steam generation [26]. Parabolic troughs are also considered for direct steam generation where the fluid in the pipe is

30

Table 1.5: Summary of the different concentrated solar receiver technologies and their operating conditions

Technology	Highest Reported Solar to Electricity Efficiency	Operating Temperatures	Most Studied Integration Method for Hybrid Cycles
Parabolic Trough	20% [33, 92]	< 670 K [33, 92]	Supplemental Heat for Steam Cycles [34, 28, 75, 106, 35, 125, 58]
Linear Fresnel Reflector	15% [65]	< 520 K [65, 73]	Supplemental Heat for Steam Cycles [74]
Central Receiver	23% [33]	850 K - 1070 K [24, 25, 26, 33, 54, 98]	Preheating Compressed Air [25, 36, 93, 62]
Solar Dish	31.25% [9]	870K - 1020 K [33]	Solar Reforming [70]

the working fluid (steam) of the power cycle [22, 73, 127]. Parabolic trough systems can also be used with different types of thermal energy storage systems such as two tank sensible heat systems, molten salt systems, phase-change systems [45, 49, 83], solid media storage systems (like concrete) [63], and steam storage [76].

The operating temperatures of these parabolic trough systems can be as high as approximately 670 K with a reported peak solar to electricity efficiency of about 20% (see Section 1.2 for a formal definition) [33, 92]. Also, due to the relative maturity and low price of this technology, a parabolic trough system is one of the more popular options for use in a hybrid combined cycle. Parabolic troughs can be used to reheat feedwater extracted from the Heat Recovery Steam Generator (HRSG), which in turn increases the flow of steam into the steam turbine allowing for more power to be produced with less fuel consumption [81]. However, due to the relatively low operating temperatures, parabolic troughs may not be as suited for use in hybrid

Brayton cycles or in solar reforming [33].

Fresnel reflectors are similar to parabolic troughs in that solar radiation heats a receiver pipe which contains the heat transfer fluid. In other words, both are line-concentrating systems. However, instead of parabolic shaped mirrors, Fresnel reflectors are long and narrow and have little to no curvature [74]. Fresnel reflectors also differ from parabolic troughs in that the reflectors are composed of several long row segments which then focus on elevated long receivers running parallel to the rotational axis of the reflectors [73]. Fresnel reflectors also tend to be cheaper than parabolic troughs (approximately 25% cheaper), however, they also tend to have lower efficiencies as well (percent differences as high as 20%) [65].

It should also be noted that even though, as previously stated, both troughs and Fresnel reflectors have relatively low operating temperatures and therefore may not be as suited for use in hybrid Brayton cycles or in solar reforming, there is current work being done with direct steam generation in troughs (described earlier) and Fresnel reflectors that can allow these line-concentrating systems to operate at temperatures as high as 773 K [22, 8]. These higher operating temperatures can potentially lead to integration methods for troughs and Fresnel reflectors beyond just preheating or reheating feedwater. However, increased costs, optical losses, and heat losses should also be potentially considered.

1.3.2 Central Receiver Systems

Central receiver systems use a field of two-axes tracking heliostats to reflect solar energy onto a single receiver or a small number of receivers. The most common configuration are solar towers, where the receiver is mounted on the top of a tower positioned at the center of or on one side of the field. A fluid is again used as the heat transfer medium. Fluids used in solar tower systems include steam/water, molten salts, liquid sodium, and air. A solar tower system also has the capability of energy storage through the use of molten salts and two tank systems [26, 96].

These solar tower systems can traditionally reach operating temperatures of up to 850 K with a reported peak solar to electricity efficiency of 23% (see Section 1.2

for a formal definition) [33]. However, research is being done on solar air-towers with pressurized volumetric receivers combined with gas turbines that can reach operating temperatures between 1020 K and 1200 K [24, 25, 26, 54, 98]. These volumetric receivers operate by having a volume within the receiver made of various materials such as ceramics, metal, and foam which absorbs the concentrated solar radiation while the working fluid goes through the volume and is heated by forced convection [15]. Recent research has also been done towards designing alternative volumetric receivers that do not require a tower (i.e., all equipment including receivers are on the ground) [42, 78, 107, 108]. With higher operating temperatures than the parabolic troughs, solar towers are usually more suited for preheating the compressed air (either directly or through a heat transfer fluid) in a hybrid Brayton or Combined cycle or, depending on the reforming method, as the heat source for solar reforming.

1.3.3 Solar Dish Systems

One of the most common solar dish systems is the dish-engine. Dish-engine systems are the most efficient of the receiver technologies in terms of the maximal achieved conversion of solar energy into electricity (see Section 1.2 for formal definition). In this system, the dish concentrator reflects solar rays onto a receiver located at the focal point of the concentrator (usually parabolic). The receiver then uses the solar energy to heat a gas (usually Helium or Hydrogen), which is then used as the working fluid in an engine, e.g., Stirling engine, to produce power [26].

The highest reported solar to electricity efficiency (see Section 1.2 for formal definition) for solar dish-engine systems is 31.25% [9]. Operating temperatures of this system can reach as high as 1020 K [33]. The dish-engine system is also the least mature of the receiver technologies and is modular in design with a single dish limited to a capacity on the order of 10-50 kW$_e$ [33]. Therefore, at least in the near-term future, solar dish-engine systems are more likely to be used in smaller, high-value applications rather than large scale hybrid power generation plants.

However, solar dishes without the engines have been used as the heat source for ammonia based thermochemical energy storage through the production of hydrogen

[70]. The solar dishes used for the thermochemical energy storage have reached operating temperatures as high as 870 K [70]. Due to the relatively high temperatures, solar dishes can be potentially be used in solar reforming systems.

1.4 Hybridization Schemes

In this section, the different hybridization schemes that have been previously proposed will be discussed. As aforementioned, the three main schemes are: solarized gas turbines, hybrid combined cycles, and solar reforming systems.

1.4.1 Solarized Gas Turbines

Modifications to Gas Turbine Systems for Hybrid Operation
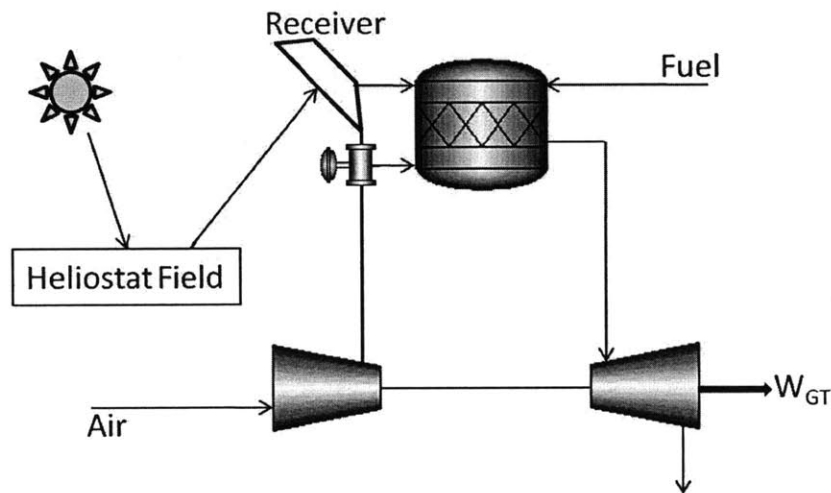
Figure 1-3: Example of hybrid solar-fossil fuel gas turbine: Compressed air is heated before entering the combustor and when solar energy is not available, the air is directly sent to the combustor

Solarized gas turbine systems use a CSP system to preheat the compressed air (to a high temperature - around 1070 K) before it enters the combustion chamber (Fig. 1-3). This increased compressed air temperature results in a reduction of fuel consumption and thus in the reduction of exergy losses (irreversibilities) in the combustion chamber.

Consequently, this integration scheme can yield higher efficiencies (see Section 1.2 for formal definition) - up to 30% when utilizing solarized gas turbines in a combined cycle [36] - if the increased operating temperature does not yield significantly higher solar to thermal losses. In particular, this arrangement can yield higher efficiencies when compared to solar energy utilized in steam generation depending on the gas turbine being used[80]. This higher solar to electric efficiency leads to a reduction in the necessary heliostat field size which, in turn, leads to an overall reduction in cost of the solar application. Also, with this integration method, the solar share (formally defined in Section 1.2) is a function of the solar receiver outlet temperature [25, 48]. This integration method also allows the power cycle to operate at full load and efficiency even when there is no solar energy available [93].

Solarized gas turbines have been both modeled and built using solar towers with different heat transfer fluids for the preheating process. Computer models of solarized gas turbines have been created for a hybrid turbine with solar preheating from a nitrate-salt solar tower [93] and turbines utilizing a solar tower with pressurized volumetric receivers for preheating. These models will be discussed in more detail in Sections 1.4.1 and 1.4.2. Maximum air preheating temperatures have reached a maximum of approximately 830 K for the nitrate-salt solar tower [93] while the preheating temperatures for the tower with pressurized volumetric receivers have gone as high as 1070 K [24]. The higher temperatures associated with the volumetric receiver tower makes it a more attractive option as the solar to electric efficiency would be higher; however, turbine modifications are required for steady operation. An actual modified gas turbine with the addition of the pressurized volumetric receivers was built and tested, and the modification process and test results will now be discussed in detail [36].

SOLGATE Project

The SOLGATE Project was started in 2002 by ORMAT industries to build a prototype of a solarized gas turbine [117, 36]. The solarized gas turbine consists of a modified 250 kW_e turbine and two pressurized volumetric receivers and one tubular receiver in series (Fig. 1-4).
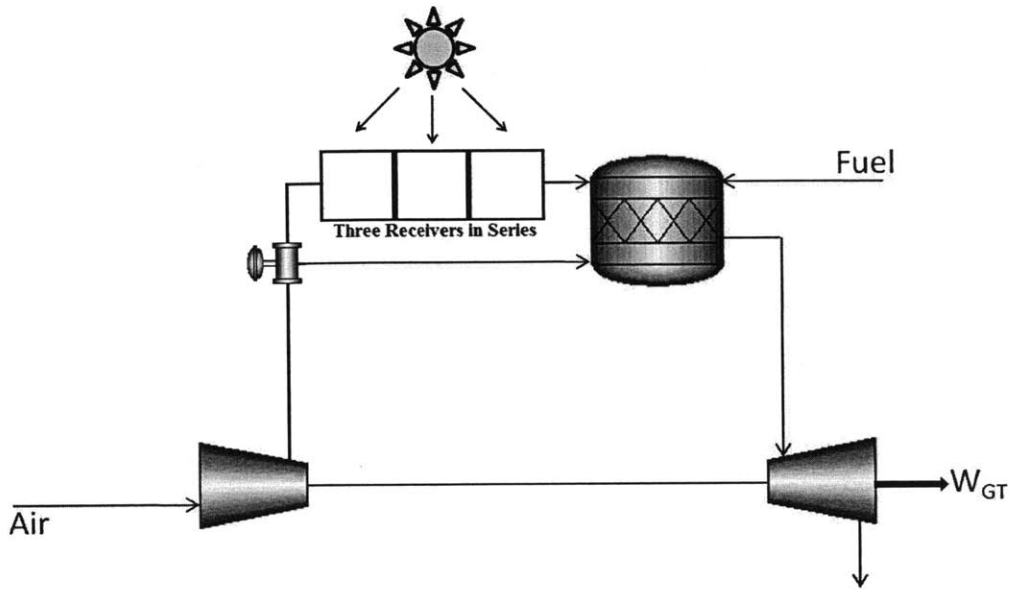
Figure 1-4: ORMAT hybrid solar-fossil fuel gas turbine schematic (adapted from [36])

The volumetric receivers consist of a volumetric absorber and a domed quartz window [24]. These receivers are tested in Spain at the Plataforma Solar de Almería (PSA) and the measured thermal efficiencies (defined as the amount of thermal energy absorbed by the receiver minus the heat losses over the amount of incident solar insolation available) of the receivers ranged from 63% to 75% with a pressure drop across the receiver of 18 mbar [25].

The issues that arise with the incorporation of the volumetric receivers include a higher combustor inlet temperature than traditional fossil-only plants and pressure drops across the receiver [36]. To overcome these issues, the combustor is redesigned with an in-line super alloy combustion chamber, a new air ducting system is added, and a nitrogen purging system is added to prevent the injector from clogging [36].

The turbine was tested at PSA with 55 heliostats focused onto the receivers delivering approximately 1 MW_{th} of solar power. The compressed air in the receiver cluster is heated from 570 K to 1080 K and the hybrid gas turbine cycle has a first law efficiency of approximately 20% (defined in Section 1.2) [36, 48].

The test shows that hybrid solar-fossil fuel gas turbine operation is conceptually

possible, however, this test was only done on a very small scale and further work needs to be done in order to have this design realized on a larger scale.

Modeling of Solarized Gas Turbine Systems

In a study done by Schwarzbözl et al. [100], two industrial gas turbine systems were chosen for technical and economic analysis as potential hybrid solar prototype plants: 1. Heron H1 - intercooled recuperated two-shaft engine with reheat and an ISO rating of 1.4MW and 2. Solar Mercury 50 - recuperated single shaft gas turbine and an ISO rating of 4.2MW.

The maximum receiver exit temperature is designed to be 1070 K and the systems are analyzed for two different locations: Daggett, California and Seville, Spain. The annual performance of the plant is calculated using the TRNSYS STEC software. A typical meteorological year on an hourly basis is used for each location. The power cycle efficiency results for 24 hour operation are shown in Tab. 1.6.

Table 1.6: Annual efficiency results for two solarized gas turbine cycles [100]

Plant	Power Cycle Efficiency (%)
Heron1 - Seville	40.4
Heron1 - Daggett	38.4
Mercury50 - Seville	35.9
Mercury50 - Daggett	35.9

The power cycle efficiencies (see Section 1.2 for formal definition) of the simulated gas turbines are comparable to traditional fossil fuel Brayton cycles (both with regeneration and without) [31, 30, 44, 124]. This comparison is made in relation to a general high efficiency gas turbine cycle rather than to the exact same gas turbine cycle without solar due to the fact that this comparison gives a better measure of the potential of the hybrid system (see discussion of reference plant in Section 1.2). Presumably in [100] the efficiencies are calculated using the first law (see the discussion on first vs. second law efficiencies in Section 1.2). Also, while this study does evaluate annual performance, the design of the plant was still based on a certain point in time rather than for an entire year.

For the economic analysis, an emerging market is assumed and the analysis covers all expenses for engineering and development of the solarized gas turbine. It is also assumed that the plant is fully operated by the staff on site. The solar field design is cost optimized using HFLCAL code [18]. The levelized electricity costs are shown in Tab. 1.7.

Table 1.7: Economic analysis results for two solarized gas turbine cycles (total cost including solar costs) [100]

Plant	LEC (€/KWh)
Heron1 - Seville	0.1913
Heron1 - Daggett	0.1993
Mercury50 - Seville	0.1004
Mercury50 - Daggett	0.0988

Solarized Steam Injection Gas Turbines

In addition to the solarized gas turbines discussed previously, there is also a solarized steam injection gas turbine where the low temperature solar heat is used to create steam which is then injected into the combustor in order to produce more power. This solarized steam injection gas turbine has yielded first law efficiencies between 40 and 55%, incremental solar efficiencies between 22 and 37%, and input solar shares of up to 50% [69]. The disadvantage of this type of gas turbine is that a low cost condenser would be needed.

1.4.2 Combined Cycles

Many studies have been done regarding hybrid solar-fossil fuel combined cycles. The main reason for this is that combined cycles have higher thermal efficiencies than either Brayton or Rankine cycles. In particular, when integrating the solar application with the gas turbine cycle, assuming a positive incremental solar efficiency (defined in Section 1.2), these higher thermal efficiencies can lead to lower capital costs for the integration of the solar application because less receiver/heliostat area would be

needed. Solar energy is typically incorporated into a combined cycle in two main ways (usually one or the other but can be both): in the gas turbines as mentioned in Section 1.4.1 or as supplemental solar heat to the bottoming Rankine cycle. There are many different solar integration configurations for the bottoming cycle, and some of the most studied methods for this type of integration in literature include preheating the steam, extracting steam from the HRSG for reheating, and increasing the flow rate of hot gas into the HRSG by supplementing the flue gas from the gas turbine with air heated by the solar application. A few hybrid solar-fossil fuel combined cycles are also currently being built in Egypt, Algeria, and Morocco [121].

Various studies have also been conducted concerning solar hybrid combined cycles with some form of CO_2 capture [53, 61, 84]. However, the focus here will be on the integration of the solar application into the combined cycle.

Comparison of Different Integration Methods

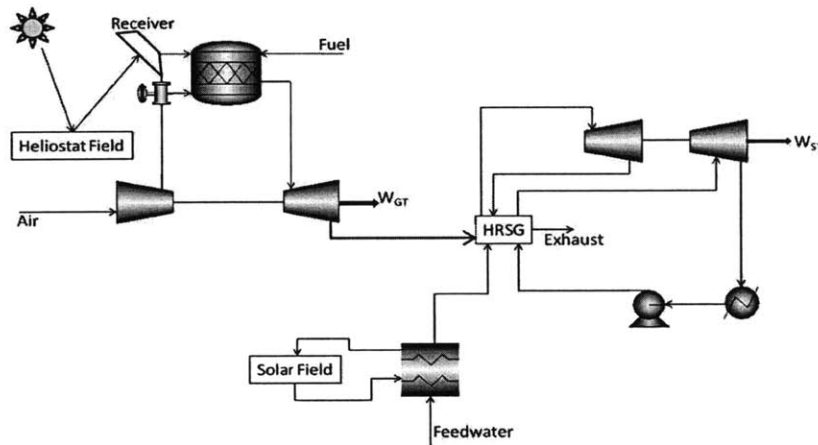Figure 1-5: Possible solar integration methods in a combined cycle: Solar heat can be added to the top cycle, the bottoming cycle (preheating the feedwater), or both (shown here)

One of the earlier studies on solar combined cycles was done in 1987, and this study did a thermodynamic analysis and comparison of three different integration methods [80]. The three different configurations compared are a cycle that incorporates both

39

the preheating of compressed air and supplemental heat to the Rankine cycle called Plant A (Fig. 1-5), a cycle with just the supplemental heat called Plant B (Fig. 1-5 without the solar preheating of air), and a cycle with just the preheating of air called Plant C (Fig. 1-5 without the solar in the bottoming cycle) - the configuration of which was first suggested in 1979 [64]. In [80], both an energy and exergy analysis was performed. The definitions for energy and exergy efficiency are discussed in Section 1.2. The overall efficiencies of all three plants, taking into account combustion, exhaust, receiver, and heat transfer losses, are shown in Tab. 1.8.

Table 1.8: Efficiency comparison for three different hybrid combined cycles (shown in Fig. 1-5) [80]

Plant	Integration Method	η_I (%)	η_{II} (%)
A	Both supplemental heat to the bottoming cycle and preheating of compressed air	26.2	27.1
B	Supplemental heat to the bottoming cycle only	29.8	30.9
C	Preheating of compressed air only	27.5	28.3

As can be seen from Tab. 1.8, Plant B has the highest efficiency while Plant A has the lowest efficiency. This result is surprising in that one would assume that at the very least, Plant C would have a higher efficiency than Plant B due to the higher second law efficiency of the solar component (42%for Plant B versus 58% for Plant C [80]). This non-intuitive result can be explained by the fact that increased combustion losses are countered by decreased heat losses. To further explain, Plant B has higher combustion losses than Plant C while Plant B has lower heat losses than Plants C (due to the high temperature heating of air). However, the lower heat losses in Plant B outweigh the higher combustion losses and therefore Plant B has a higher overall cycle efficiency than Plant C[80].

Because Plant B has a higher overall efficiency many studies have looked at different configurations of using solar as supplemental heat to the steam cycle and those studies will be discussed in more detail in Section 1.4.2. On the other hand, due to the higher efficiency for the solar component in Plant C, the cost of the solar application can be reduced, which also makes the Plant C configuration a viable integration

method. Therefore, in order to truly determine which configuration is more suitable, [80] suggested an economic analysis should be done in addition to a thermodynamic one.

Since the publication of [80], many improvements have been made in terms of turbomachinery (higher allowed inlet temperatures and better isentropic efficiencies) and combined cycle configuration (use of reheat) [29]. All of these improvements lead to higher efficiencies which means that calculated efficiencies of current cycles will be higher than the ones calculated in [80]. However, the efficiency comparison would most likely be the same because both gas turbine and steam turbine technologies have improved since [80] was published.

Combined Cycle with Solar Integration in Gas Turbine

SMUD Kokhala Study [93]

In 1996, NREL and the Sacramento Municipal Utility District (SMUD) conducted a conceptual evaluation of a 30.5 MW_e combined cycle plant that uses a nitrate-salt solar tower with a salt/air heat exchanger to heat the compressed air at the gas turbine combustor inlet during peak solar insolation conditions.

The combined cycle uses a Westinghouse WR 21 gas turbine and due to the lack of design data, the cycle design configuration is developed by the GateCycle program. The cycle has a design point solar contribution of $18MW_t$ or approximately 27% of the total thermal input to the gas turbine.

Eight different solar plants ranging from 10 to $70MW_t$ were designed for the integration with the combined cycle. All the solar plants use a Solar-Two type nitrate-salt external receiver with a solar field of $50m^2$ heliostats. The DELSOL3 computer code [59] is used to design the receiver diameter and height, tower height, and number of heliostats for lowest energy costs. The location for the design is Daggett, California, and the design uses a constant direct normal insolation of $950W/m^2$.

The annual thermal performance of the solar plants were modeled using SOLERGY [115]. Although SOLERGY is most often used to calculate electricity output, in [93], it was used to determine the thermal delivery of the solar plant to the com-

bined cycle. A spreadsheet model was developed to evaluate the combined cycle. Thermal values from SOLERGY are imported into the model every 15 minutes and then the model calculates the annual electric production level supported by the solar input. Natural gas is then allocated to support this level of operation in order to achieve the 90% annual capacity target. An economic analysis is performed. The heliostat costs are assumed to be $250/m^2 and all other costs, including capital, O&M, receiver and plant equipment costs, are based on existing solar and combined cycle plants. The economic and thermal analysis results are shown in Tab. 1.9.

Table 1.9: SMUD Kokhala thermal and economic analysis results for a solarized gas turbine combined cycle [93]

Solar Plant Size [MW$_t$]	50
Thermal Storage [MWh$_t$]	423
Annual First Law Efficiencies	
Heliostat Field	.562
Receiver	.791
Storage	.983
Salt Heat Exchanger	.999
Total Solar	.437
Gross Solar to Electric	.203
Net Solar to Electric	.196
Economics	
LEC [$/kWh]	0.048
SLEC [$/kWh]	0.068

The results are given in terms of annual performance, however, the design is still based on a certain point in time (i.e., one insolation value) rather than for an entire year (i.e., taking into account fluctuating solar supply in design phase).

The focus of the SMUD Kokhala study is the efficiency of solar to electric conversion, which for hybrid systems is the incremental solar efficiency (defined in Section 1.2), rather than the overall cycle efficiency. While the incremental solar efficiency is

42

important when evaluating a configuration, it should be evaluated in conjunction with the cycle efficiency in order to take into account the usage of fuel and to determine the true performance of the plant.

Kribus et al. Study [62]

Kribus et al. [62] also analyzed a combined cycle with solar heating of the compressed air in the Brayton Cycle. The difference compared to [93] is that instead of using a nitrate-salt solar tower with a heat exchanger, a Solar Concentration Off-Tower (SCOT) and high temperatures receivers is used. The SCOT is different from a traditional solar tower in that there is a reflector atop the tower which redirects the solar radiation towards a focal region near ground level.

The hybrid solar combined cycle is designed using a modified DELSOL3 program called WELSOL. WELSOL adds a SCOT optic model and additional options for receivers, hybrid operation, and power generation to the DELSOL3 code. In addition, the WELSOL code includes calculation of losses due to the additional optical elements, models of the performance of the high temperature receivers, gas turbine and combined cycle performance models, and cost models for new components (i.e., additional reflectors, receivers, etc.).

Using WELSOL, the system is designed for the lowest LEC; however, in order to improve computation speed, the physical models used in the WELSOL code are simplified. To more accurately simulate the performance of the systems, two other codes are used to simulate the system and these results from the more-detailed simulation are used to validate the performance predictions of the optimized systems generated from WELSOL. For the more-detailed simulation, the optics are simulated using a statistical ray-tracing code called WISDOM [101] and then the output of the optics simulation are used as input in the thermal analysis code ANN, which simulates the performance of receivers, power conversion systems, and annual integration.

In [62], two SCOT/Combined Cycle (CC) systems are presented: a 600 kW$_e$ system and a 34 MW$_e$ system. The location used for the study is Barstow, California. The LEC is calculated to be between \$0.05/kWh to \$0.10/kWh depending on plant capacity factor for the 34 MW$_e$ system and between \$0.10/kWh to \$0.20/kWh de-

pending on plant capacity factor for the 600 kW$_e$ system. Other results from the optimization of the SCOT/CC system are shown in Tab. 1.10.

Table 1.10: Layout of lowest LEC SCOT system for integration with a combined cycle [62]

Plant Rating	0.6 MW$_e$	34 MW$_e$
Number of Heliostats	48	1323
Tower Height [m]	49	163
Tower Reflector Area [m^2]	190	3270
Turbine Inlet Temperature [K]	1273	1473
Gross Power Conversion Efficiency	.356	.470
Annual Solar to Electric Efficiency	.161	.213
Solar Capacity Factor	.220	.242
Specific Cost [$/kW]	3943	2588

The performance calculations are based on an energy analysis as opposed to an exergy analysis (see discussion in Section 1.2). [62] also suggests a size optimization study should be performed in order to determine the optimal size of a SCOT plant that can be implemented with a combined cycle.

Other Studies

Another study done by Segal and Epstein optimizes a combined cycle with a solarized gas turbine for maximum efficiency [103] with a focus on determining the best solar receiver temperature for efficiency. The efficiencies for a hybrid solar-fossil fuel combined cycle range from 35% to 55% for solar receiver temperatures between 1000 K and 2000 K [103]. However, receiver temperatures of 2000 K are most likely unrealistic as the highest reported receiver temperature is approximately 1300 K with realistic operating temperatures around 1100 K [24].

Kakaras et al. [56] considered a combined cycle with wet gas turbine technologies which uses the solar heat to evaporate water injected into the compressed air before it enters the combustion chamber [56]. Although this cycle shows improvements for both efficiency and cost on a small scale, [56] concludes that it is not likely to be

applied on a large scale due to the increased cost.

Combined Cycle with Solar Integration in Steam Cycle

Many different studies have looked at the integration of solar into the steam cycle of the combined cycle in a variety of ways. An economic analysis for Egypt was performed on two different hybrid combined cycles. The first cycle analyzed uses a parabolic trough system to preheat a fraction of the feed water in a solar boiler, and the second cycle uses a solar-air tower to heat air to temperatures higher than those of the exhaust gas from the gas turbine and then the heated air is mixed with the exhaust gases before entering the HRSG. While the economic analysis found a LEC comparable to the LEC of a traditional fossil fuel plant, the solar share that produces this LEC is not given, so it is unclear if this low LEC includes a significant solar share.

The integration method of mixing solar-heated air with the exhaust gas of the turbine before it enters the HRSG has also been considered for cogeneration power plants [14].

Another study done in California also analyzed a CC with a parabolic trough system that preheats some of the feedwater [34]. A duct burner is used as backup when solar energy is not available. The efficiencies for the plant and solar shares (defined in Section 1.2) for various situations are shown in Tab. 1.11. This study is one of the few where both design and performance evaluation takes into account fluctuating solar supply.

Table 1.11: Performance of combined cycle in California for different operation modes [34]

Solar/Duct Capacity [%]	100/0	50/0	50/50	0/100
Steam Cycle Efficiency [%]	37.5	36.72	36.98	37.61
Solar Share [%]	17.57	9.32	4.08	0
Fuel Based Net Electric Efficiency [%]	66.42	62.21	58.80	52.23

An exergy and energy analysis was also performed on a hybrid solar combined cycle in Yzad, Iran [16]. In this case, the solar energy is used to reheat extracted feedwater

from the HRSG. The steady state analysis is performed for June 21 at noon in Yzad with a solar radiation of approximately 800 W/m^2. Ideal gas mixture principles are assumed for the combustion products and heat losses are only considered for the collectors and solar heat exchangers. The first and second law efficiencies (defined in Section 1.2) are calculated to be 46.17% and 45.6%, respectively [16]. These two efficiencies are relatively close because the exergy of the solar and fuel input are approximately equal to the energy of the solar and fuel input (see Section 1.2).

The fact that this analysis only evaluates the cycle at one point in time rather than over a 24 hour period or over a year means that the fluctuating solar supply, which has a great impact on the efficiency, is not taken into account. Since the efficiency for this Iran study is calculated for when the solar irradiation is the highest, the reported efficiencies are presumably the highest possible efficiency rather than an overall average efficiency.

There have also been studies done to determine the best method of solar integration within the steam cycle. In a study done by Odeh et al. three different methods of solar integration (boiling, preheating, and preheating boiling) into a steam cycle (Fig. 1-6) are compared based on the amount of fuel consumed [81].

The boiling process arrangement is where the solar collector field is connected in parallel with the boiler of the steam cycle. The preheating process arrangement has the collector field in parallel with the feedwater heaters of the steam cycle and the collector field has the same inlet and exit temperatures as the feedwater heaters. The preheating boiling process arrangement is a combination of the boiling and preheating arrangement in that the collector field is connected in parallel with both the boiler and the feedwater heaters in the steam cycle. The amount of fuel is calculated in terms of kilogram of fuel needed per kWh produced. These results show that the boiling configuration is the best configuration in terms of fuel savings and therefore would have the highest increment CO$_2$ avoidance [81].

There are also many other studies on combined cycles with the solar heat applied to the steam cycle, including ones in California [28], Australia [75], Spain [106], Libya [35], China [125], and Tunisia [58], making solar integration into the steam cycle

46

Boiling Process (Fixed Turbine Output)

Preheating Process (Variable Turbine Output)

Preheating Boiling Process (Variable Turbine Output)
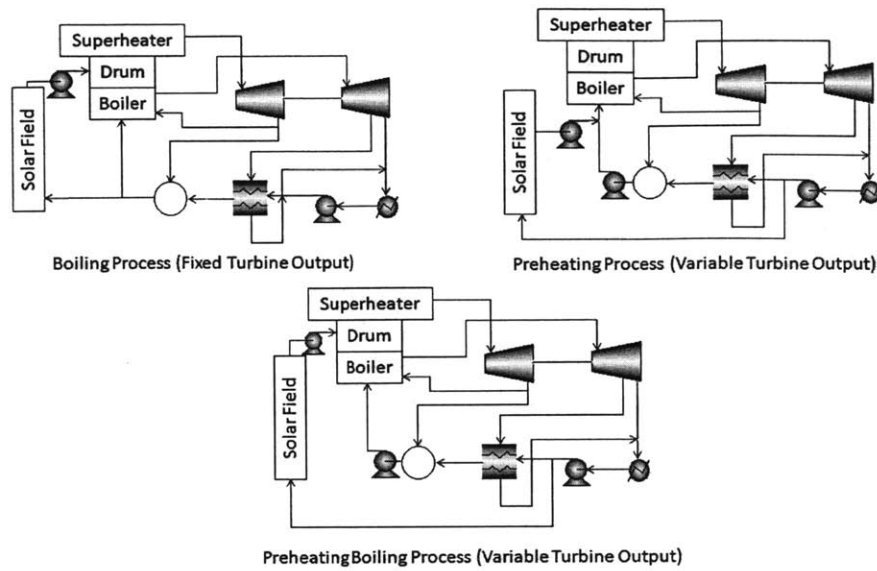
Figure 1-6: Three different solar integration methods in the steam cycle (adapted From [81])

one of the more previously studied areas of hybrid solar power generation. A list of currently existing hybrid combined cycles is shown in Tab. 1.12. However, while some studies do give annual performance results, when it comes to the design of the hybrid plant, most of the previous research done does not take into account a time dependence of solar input and plant revenue due to the variation in electricity prices.

1.4.3 Solar Reforming

Figure 1-7: General schematic of solar reforming

Solar reforming (Fig. 1-7) is one of the most promising methods of integration

Table 1.12: Currently existing hybrid solar-fossil fuel combined cycles [121]

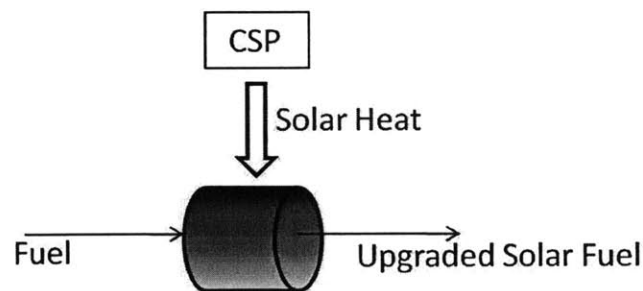| Project Name	Location	Solar Technology Used	Total Output (MW$_e$)	Solar Contribution (MW$_e$)	Status
Kuraymat	Egypt	Parabolic Trough	140	20	Operational[10]
Victorville	California	Parabolic Trough	563	50	Planned[4]
Palmdale	California	Parabolic Trough	555	62	Planned[3]
Hassi R'Mel	Algeria	Parabolic Trough	130	25	Operational[7]
Yazd	Iran	Parabolic Trough	430	67	Operational[6]
Martin	Florida	Parabolic Trough	3705	75	Operational[5]
Agua Prieta	Mexico	Parabolic Trough	480	31	Planned[17]
Ain Beni Mathar	Morocco	Parabolic Trough	472	20	Operational[1]

because it allows for energy storage. While a hybrid system does not necessarily need storage because fuel is available when needed, this added storage allows for the use of stored solar instead of fuel when no solar is available which possibly leads to higher solar shares (or a higher reduction in fuel usage). Using concentrated solar radiation as the high temperature heat source provides a process of converting solar energy into chemical energy, which can either be used immediately for power generation or stored for later use when solar energy is not available [114].

Solar Thermochemical Processes

Solar thermochemical processes can be used to upgrade traditional fossil fuels, but these processes still face many challenges such as the design of the catalyst and reactor. One of the most studied solar thermochemical processes is steam reforming [50, 51, 82, 91, 104, 110, 112, 113, 116, 129]. This process is a catalytic reaction between hydrocarbons such as methane with steam. The product of this reaction is mainly a mixture of CO and H_2 called synthetic gas or "syngas". The basic steam

reforming reaction for methane is:

$$CH_4 + H_2O(l) \rightarrow CO + 3H_2$$
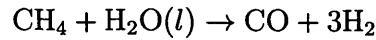
In some cases, the water gas shift reaction (shown below) may also be important.

$$H_2O + CO \rightarrow CO_2 + H_2$$
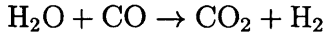
Steam reforming of methane is a prime candidate for the conversion of high temperature solar heat to chemical fuels because equilibrium conversion is greatest at high temperatures and low pressures. For instance, at a pressure of 1 atm the equilibrium conversion of methane exceeds 90% at 1000K. This process is highly endothermic ($\Delta H^o_{rxn} = 205$ kJ/mol) [119] and can improve the calorific value of the methane feed by as much as 28% [60]. In addition, with solar reforming, the energy is stored in chemical form which would most likely be more compact than traditional thermal energy storage systems and would be much cheaper than storing electricity. Other solar thermochemical processes have also been studied such as steam or CO_2 gasification of coal [116, 129, 130, 88].

System Integration

One approach to integrating the solar reforming system with the power generation system is to have the solar system operate independent of the power generation system, meaning that the power cycle can still run even if the solar reforming system is not running and vice versa. For this proposed schematic, after the syngas leaves the solar reformer it is used for heating and evaporating the steam needed for the solar reforming process. The cooled down syngas is then fed into the combustion chamber of the gas turbine as a fuel. Advantages of this method are that only minor modifications need to be made to traditional power generation systems like combined cycles or gas turbines and existing power generation systems can be easily retrofitted with the reforming system. A proposed schematic is shown in Fig. 1-8, and it is claimed that this system configuration can yield fuel savings of up to 25% (as compared to a

cycle using methane) [119].
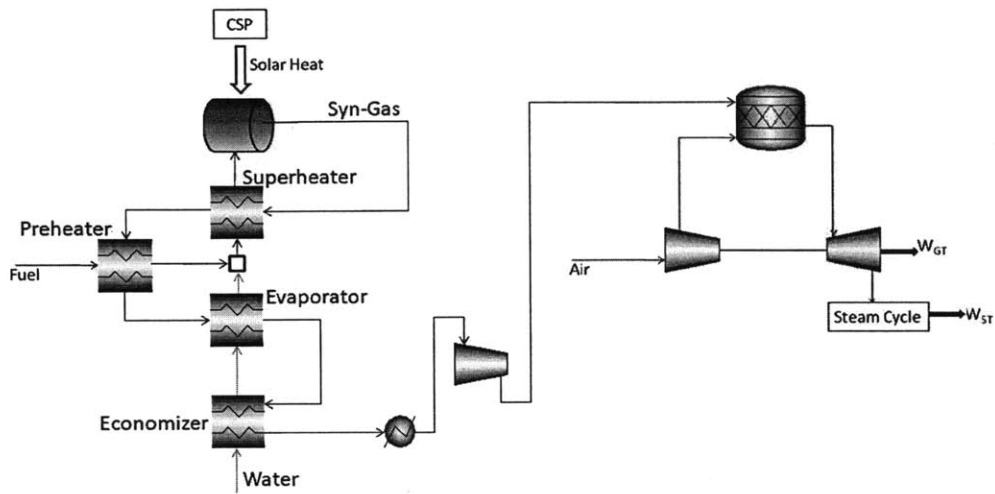
Figure 1-8: Schematic of solar syngas fired power plant (adapted From [119])

While this integration scheme is promising, some disadvantages include the need for the storage of gases and the fluctuation of reforming capacity from day to day unless a thermal storage system is added.

Low/Mid Temperature Cycles

While most hybrid power cycles with solar reforming require high temperatures from the solar input in order to carry out the reforming reaction, a few cycles have been proposed that only require low or middle solar input temperatures.

One cycle that uses middle temperature solar heat is the one proposed by Hong et al. [52] where solar input in the 470-570 K range is used for methanol reforming. The syngas created from the reforming reaction is then sent to the power cycle (a combined cycle) as the fuel input. The cycle is simulated in Aspen Plus and the second law efficiency, solar share, and net incremental solar efficiency are found to be 60.7%, 18%, and 35%, respectively.

Another cycle that uses low/mid temperature solar heat is the SOLRGT cycle [131]. The SOLRGT cycle uses low/mid temperature solar heat and integrates it with an intercooled chemically recuperated gas turbine (CRGT) system. A schematic is shown in Fig. 1-9.
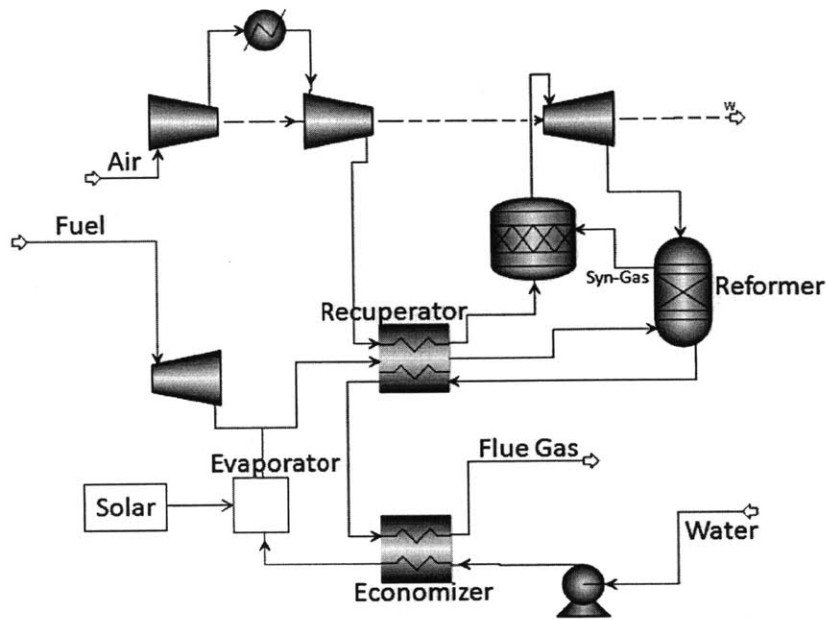
Figure 1-9: Schematic of SOLRGT cycle (adapted from [131])

A traditional CRGT system uses a HRSG to recover the turbine exhaust gases. The superheater of the HRSG is replaced with a steam reformer and the reforming process uses the turbine exhaust as the heat source to produce syngas. In the SOL-RGT system, low temperature solar heat (470 K−570 K) is used to evaporate water to generate steam needed for reforming. The steam and fuel are then sent to the reformer for the production of syngas which is used as the working fluid of the CRGT system. One of the main advantages of this system is that only low temperature solar heat is needed whereas with other solar reforming systems high temperature solar heat is needed which current solar technologies may not be able to meet.

In [131], the turbine is modeled after the cooled turbine model presented in [11] and the system is simulated using Aspen Plus. The RK-Soave thermodynamic model is selected for thermal property calculations and the Gibbs Reactor is used to model the reformer. The Gibbs Reactor determines equilibrium conditions by minimizing Gibbs free energy. From the simulation, the thermal efficiency is 45.9%, the solar share is 20.3%, and the incremental solar efficiency is 26.5%. The definitions of these different metrics are discussed in Section 1.2.

The calculated efficiencies show great promise when compared to traditional CRGT systems. However, in the system efficiency definition, instead of using the exergy of the solar and fuel as inputs, the exergy of the solar and the energy of the fuel is used. However, as stated before, the exergy of the fuel is approximately equal to the energy of the fuel (see Section 1.2), so the final efficiency value would not be significantly affected. Also, no economic analysis is done.

1.4.4 Quantitative Comparison Using Proposed Linear Combination Metric

Now to compare some of the previously discussed schemes, LEC versus CO_2 emissions for a few hybrid plants are shown in Fig. 1-10.
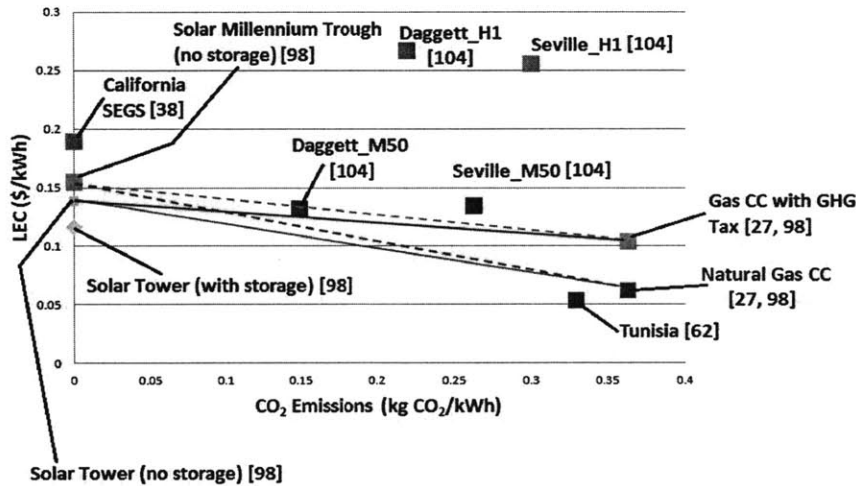
Figure 1-10: Trade off comparison between LEC and CO_2 emissions for various power plants (Tunisia LEC includes subsidy for solar)

As stated before, it is more informative to compare different metrics simultaneously in order to correctly include the trade offs associated with hybrid solar fossil fuel plants. In Fig. 1-10, a variety of solar only plants are shown along with several hybrid plants and natural gas CCs (with and without taxes for greenhouse gas (GHG) emissions). For the linear combination metric, you want to take Solar Millennium Trough and the Solar Tower with storage as your solar technologies as this is the lowest cost

52

available for the trough technology and tower technology, respectively. If you take the solar tower with storage as your currently existing solar technology, then based on the linear metric described in Section 1.2, it can be seen from Fig. 1-10 that only the Tunisia hybrid plant [58] should be considered since a linear combination (solid lines) of Solar Tower with storage [94] and Gas CC (with or without GHG tax) [94, 23] can achieve the same CO_2 emissions as the other four hybrid plants with a lower average LEC. On the other hand, if you take the Solar Millennium trough as your currently existing solar technology, then based on the linear combination metric, in addition to the Tunisia plant [58], the Daggett_M50 plant [100] could also be considered viable if taking into GHG taxes for fossil fuel only plants (see dashed blue line). It should be noted that the LEC for the Tunisia plant includes a subsidy for the solar application, so therefore it is possible that with a solar subsidy the other hybrid plants could be considered viable as well. Another point to make is that since the LECs reported do not capture time of demand, plants with high LECs but proper storage may be viable as well.

1.5   Conclusion

Overall much research has been done in combining solar energy with traditional fossil fuel power generation systems because it can lead to a decrease in fuel usage and reduced CO_2 emissions without the supply issues that are associated with pure solar thermal plants without storage. However, the main conclusion from this review is that while some studies report annual performance results, almost no studies base the hybrid plant design on time interval data. To further explain, hybrid plants should not only be evaluated using annual metrics such as incremental solar efficiency or increment CO_2 avoidance, but they should also be designed based on annual data (e.g., solar insolation over an entire year and not just for a certain design hour). By both evaluating and designing the hybrid cycle based on annual metrics, a hybrid solar-fossil fuel cycle with better performance can be determined. In addition, much of the previous work has only analyzed hybrid cycles using one metric (e.g., only looking

at efficiency or cost or emissions) or reported various metrics without showing the tradeoff between them. However, it may be more insightful to evaluate two metrics simultaneously using the linear combination metric discussed in Section 1.2. This linear combination metric can be seen as a generalization of the notion of Pareto-optimal plants (as discussed before in Section 1.2.2) and allows for the comparison between the proposed hybrid cycle and the current fleet of power plants available. This comparison gives a more conclusive determination of the viability of the proposed hybrid cycle.

Chapter 2

Hybrid Solar-Fossil Fuel Plant with Steam Reforming of Methane as Solar Integration Method

2.1 Introduction

As discussed in Chapter 1 [105], one potential solution to overcoming intermittency and cost issues associated with solar energy is hybrid concentrated solar-fossil fuel power generation. Also discussed in Chapter 1 [105] is that existing and proposed hybrid power generation processes can be grouped into three main areas: solarized gas turbines, hybrid combined cycles, and solar reforming. Solar reforming, in particular, is one of the more interesting integration methods because it allows for energy storage in the form of fuel which can be more compact and cheaper than storing electricity. While a hybrid system does not necessarily need storage because fuel is available when needed, this added storage allows for the use of stored solar instead of fuel when no solar is available which possibly leads to an even higher reduction in fuel usage when compared to a hybrid cycle with no storage. In addition, the syngas produced by the solar reforming process is considered a cleaner fuel than natural gas, which means that by combusting syngas instead of natural gas, there is the potential to reduce

emissions when compared to other hybrid cycles that utilize natural gas.

Solar reforming as the integration method for a hybrid cycle is further investigated based on the aforementioned advantages of the solar reforming integration method and also because it is the least studied integration option in the literature. The solar reforming process can, in principle, be integrated with a number of concentrated solar technologies. In this work, integration with either a parabolic trough or a solar tower is considered. In the case of the trough reformer, the reformer system is analyzed on its own and it is demonstrated that it is not a viable option. In the case of the reforming with a tower, the solar reformer system is also integrated with a combined cycle in order to optimize the design and operation of a hybrid solar-fossil fuel plant using solar reforming.

2.2 Parabolic Trough Reforming

First, the integration of solar reforming with a parabolic trough will be discussed.

2.2.1 Model Description

The trough model is based on the Sandia model [37]. The trough model is created in Aspen Custom Modeler® and then implemented with a steam reforming model in Aspen Plus®.

Parabolic Trough Model

As discussed in Chapter 1 [105], a trough uses a single-axis tracking curved mirror system to concentrate solar radiation onto a receiver pipe through which a heat transfer fluid (HTF) flows. Herein, the trough is represented by a steel pipe with a glass cover. Vacuum conditions are assumed between the glass cover and pipe as shown in Fig. 2-1. The model takes as inputs the solar DNI, area of solar collection, environment parameters (i.e., temperature, wind speed, etc.), HTF parameters (inlet temperature and pressure, flow rate, density, heat capacity, and viscosity), and trough parameters (length, material properties, diameter of pipe, etc.) and outputs

the outlet temperature and pressure of the HTF. In order to calculate the outputs, the model first calculates the optical efficiency to determine the amount of energy actually absorbed by the pipe. Then the model discretizes the pipe into equally sized elements and a steady state energy balance is performed on each element (taking into account convection and conduction) in order to determine the outlet temperature of each element. The pressure drop across each element is then also calculated.
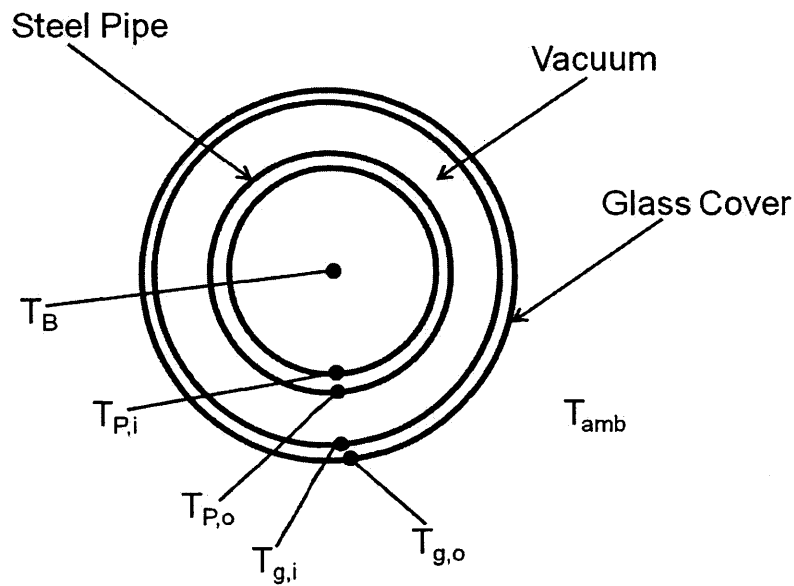
Figure 2-1: Cross-section of Parabolic Trough Receiver

The optical efficiency is calculated using several optical parameters and the incidence angle of the sun (θ). The incidence angle is defined as the angle between the sun's rays and the normal line of the parabolic mirror. The formula for the optical efficiency is as follows:

$$\eta_o = e_1\, e_2\, e_3\, e_4\, e_5\, e_6\, \rho_{cl}\, K\, \tau$$

where e_1, e_2, e_3, e_4, e_5, and e_6 are various optical parameters defined in Tab. 2.1, ρ_{cl} is the clean mirror reflectance, τ is the transmittance of the glass cover, and K is the incident angle modifier. The incident angle modifier K is calculated using the

following equation:

$$K = \cos(\theta) + 0.000884\theta - 0.00005369\theta^2$$

Table 2.1: Optical parameters for calculation of optical efficiency [37]

Parameter	Description	Value
e1	Shadowing parameter	.974
e2	Tracking error	.994
e3	Geometry error	.98
e4	Dirt on mirror parameter	reflectivity of clear mirror$/\rho_{cl}$
e5	Dirt on receiver parameter	$\frac{1+e4}{2}$
e6	Random error	.96
ρ_{cm}	Reflectivity of clear mirror	.88
ρ_{cl}	Clean mirror reflectance	.935
τ	Transmittance of glass cover	.935

The amount of energy absorbed by the pipe is then equal to:

$$\dot{Q}_{abs} = q \, A \, \alpha \, \eta_o$$

where q is the DNI, A is the total area of collection, α is the absorptance of the pipe, and η_o is the optical efficiency calculated. Once the optical losses are taken into account, the energy balance for each individual element is performed based on the thermal resistance network shown in Fig. 2-2. In the resistance network, T_B is the bulk temperature of the HTF, $T_{P,i}$ is inner wall temperature of the pipe, $T_{P,o}$ is outer wall temperature of the pipe, $T_{g,i}$ is the inner wall temperature of the glass cover, $T_{g,o}$ is the outer wall temperature of the glass cover, and T_{amb} is the environment temperature. The temperatures are also shown schematically in Fig. 2-1.

Figure 2-2: Trough Model Resistor Network

The resistances in the network are calculated using standard methods. The Nus-

selt numbers for the convective resistances are calculated using the correlations shown in Tab. 2.2.

Table 2.2: Nusselt number correlations for the convective resistances

Convective Resistance	Correlation Used
Between heat transfer fluid and pipe	Gnielinski
Between pipe and glass cover	Free-molecular convection [37]
Between glass cover and environment	Churchill and Berstein (forced convection)

Based on this resistor network, the outlet HTF temperature can be calculated using the following equations:

$$\dot{m}c_p \frac{dT_B}{dx} = \frac{T_{p,i} - T_B}{R_{conv,htf-pipe}}$$

$$\dot{Q}_{abs} = \frac{T_{p,i} - T_{amb}}{R_{rest}}$$

where $\dot{m}$ is the mass flow rate of the HTF, c_p is the heat capacity of the HTF, T_B is the bulk temperature of the HTF, $R_{conv,htf-pipe}$ is the convective resistance between the HTF and the inner pipe wall, and R_{rest} is the sum of all the resistances in the network shown in Fig. 2-2 except for $R_{conv,htf-pipe}$.

In discretized form, the equations become

$$\frac{T_{p,i,j} - T_{amb}}{R_{rest}} = \dot{Q}_{abs}/N$$

$$\frac{T_{p,i,j}}{R_{conv,htf-pipe}} = \dot{m}\, c_p \left(T_{B,j} - T_{B,j-1} \right)$$

where j refers to the discretization element and N is the number of discretization elements.

The pressure drop is calculated using the friction factor from the Zigrang and Sylvester correlation as follows:

$$\frac{1}{\sqrt{f}} = -2\log\left[\frac{k}{2.7D} - \frac{5.02}{Re}\log\left(\frac{k}{3.7D} - \frac{5.02}{Re}\log\left(\frac{k}{3.7D} + \frac{13}{Re} \right) \right) \right]$$

59

$$\Delta P = f \frac{L}{D} \frac{\rho V^2}{2}$$

where f is the friction factor, k is the thermal conductivity of the pipe, D is the inner diameter of the pipe, Re is the Reynolds number, L is the pipe length, ρ is the density of the HTF, and V is the velocity of the HTF.

Steam Reforming Model

The steam reforming model is implemented in Aspen Plus®, and the flowsheet of the steam reforming model (with the trough model created in Aspen Custom Modeler®) is shown in Fig. 2-3.
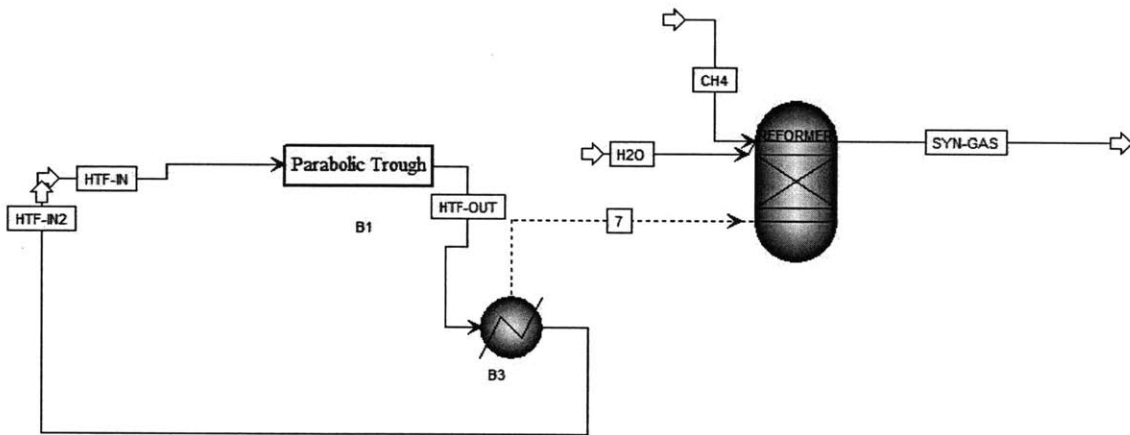
Figure 2-3: Steam reforming model in Aspen Plus®

The solar reforming system model is pseudo steady state and does not take into account storage. The solar reformer is modeled as an equilibrium reactor (a Gibbs reactor in Aspen Plus®). The equilibrium reactor calculates the outlet stream properties by minimizing the Gibbs free energy. The HTF used in the trough model is Therminol VP-1, which is commonly used synthetic oil for heat transfer. To link the reformer to the trough, the amount of energy needed to cool the outlet of the trough back to its original temperature is calculated and then inputted into the reformer as the amount of heat input. In addition to the heat input from the trough model, the reformer also has two stream inputs: methane and water. The operating pressure of

the reformer is fixed at 1 bar. The flow rate of methane is fixed and the amount of solar energy into the trough is such that the input solar share is approximately 10%. Recall from Chapter 1 [105] that the input solar share is defined as

$$X_{s,i} = \frac{\dot{Q}_{solar}}{\dot{Q}_{fuel} + \dot{Q}_{solar}}$$

so therefore the amount of solar energy can easily be determined given the fixed fuel input and fixed input solar share. The reformer outlet temperature is fixed such that it is equal to the outlet temperature of the parabolic trough in order to prevent temperature crossover. The water flow rate into the reformer is then calculated based on this fixed reformer outlet temperature. There is an obvious limitation to this temperature crossover prevention method in that the temperature crossover does not necessarily have to occur at the outlet of the reformer. However, this simplification (which represents the highest reforming temperature possible) is acceptable because as will be discussed next, the results show that even with this simplification the reforming temperature is not high enough for viable reforming.

2.2.2 Simulation Results

The reformer system is simulated using the various parameters shown in Tab. 2.3. The results of these simulations will now be shown and discussed.

Table 2.3: Parabolic trough parameters for simulation

Parameter	Symbol	Value
Environment temperature	T_{amb}	300 K
Thermal conductivity of air	k_{air}	.024 W/m-K
Wind Speed	V_{wind}	2 m/s
Thermal conductivity of glass cover	k_{glass}	.109 W/m-K
Thermal conductivity of pipe	k_{pipe}	.43 W/m-K
Outer diameter of pipe	$D_{p,o}$	.07 m
Inner diameter of pipe	$D_{p,i}$	.066 m
Outer diameter of glass cover	$D_{g,o}$	.115 m
Inner diameter of glass cover	$D_{g,i}$	.109 m
Absorptance of pipe	α_{pipe}	.94

Parabolic Trough Model Simulation Results

The trough model was simulated for different times throughout the day (i.e., different incidence angles). While the amount of q is changing, the input solar share is fixed so the required area of solar collection is varying. The solar to thermal efficiency of the trough varies between 15 and 60%. Fig. 2-4 shows how the outlet temperature of the trough varies greatly with the incidence angle. The inlet temperature is fixed at 300 K.
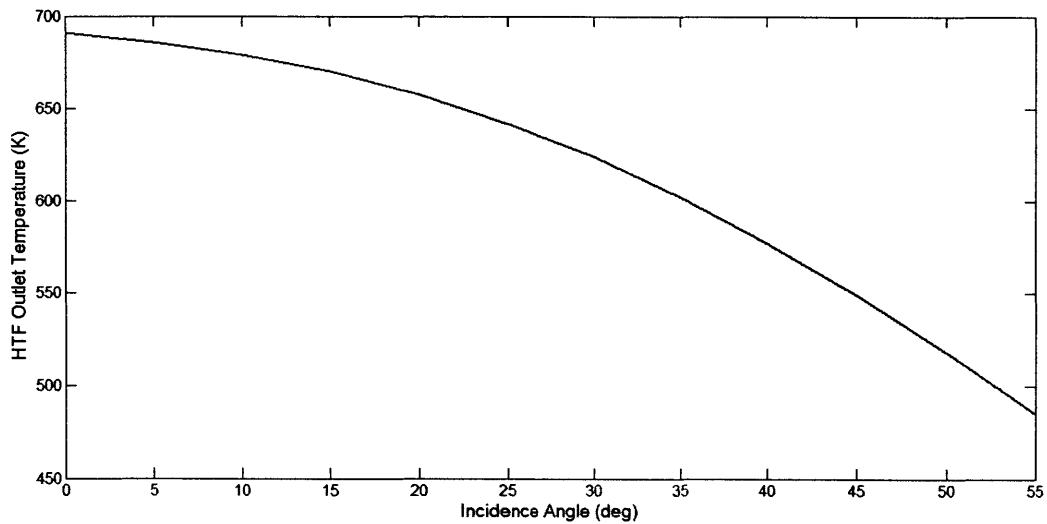
Figure 2-4: Trough outlet temperature vs. incidence angle

Steam Reforming Model Simulation Results

Again, the steam reforming model is simulated for different times through out the day (i.e., different incidence angles and therefore different outlet temperatures). Of particular interest in these simulations is the amount of water needed for the reformer in order to prevent temperature crossover at the reformer outlet. Fig. 2-5 shows the input water to fuel ratio for different reformer outlet temperatures.

As can be seen from Fig. 2-5, excessively large amounts of water are needed in order to reach the desired reformer outlet temperature and prevent temperature crossover. Based on the amount of water needed for the reforming and essentially

Figure 2-5: Input water to fuel ratio for various reformer outlet temperatures
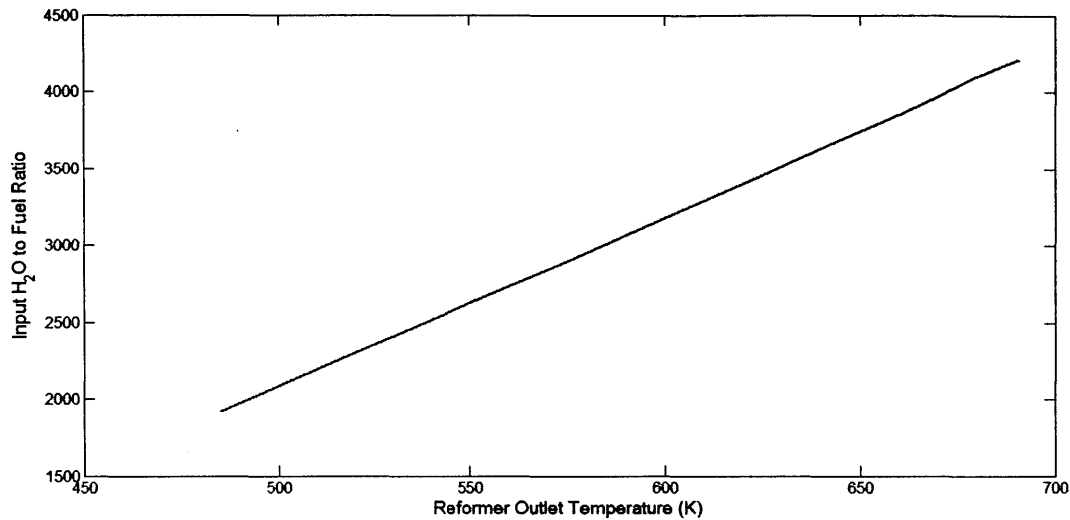
full conversion of methane, the outlet mole fraction of hydrogen and carbon dioxide are, as expected, quite low with the mole fraction carbon monoxide negligible. The mole fractions of the hydrogen and carbon dioxide only change with differing reformer temperature because of the different amounts of water needed.

Based on the simulations results, a first law analysis is performed to determine the amount of energy needed for the three main processes occurring in the reformer: the actual reforming, the heating of the methane to the reformer operating temperature, and the heating/evaporating of the water. Tab. 2.4 shows the percentage of the reformer heat input used for each process. From Tab. 2.4, it can be seen that most of the energy input into the reformer is being using for the heating/evaporating of the water, and the reformer acts primarily as a steam generator.

In essence, parabolic troughs are not suitable for solar steam reforming of methane because of the relatively low operating temperatures. Substantially higher temperatures are required to reduce the water amount. Therefore, the parabolic trough is more ideally suited for a lower temperature integration method (e.g., in a steam cycle as discussed in Chapter 1 [105]), and for solar reforming, a technology that can reach higher operating temperatures (e.g., tower) would be more desirable. It should be also noted that troughs could be used with solar reforming processes that do not

63

Table 2.4: Energy breakdown for different processes in reformer

Reformer Temperature (K)	% of Energy - Heating Methane	% of Energy - Heating/Evaporating Water	% of Energy - Reforming
485	7.75e-3	99.8	.179
518	7.70e-3	99.8	.150
549	7.67e-3	99.9	.129
577	7.64e-3	99.9	.114
602	7.61e-3	99.9	.103
624	7.59e-3	99.9	.095
642	7.54e-3	99.9	.089
658	7.53e-3	99.9	.084
670	7.50e-3	99.9	.080
679	7.46e-3	99.9	.078
686	7.46e-3	99.9	.076
691	7.47e-3	99.9	.075

require as high of temperature such as methanol decomposition [52] or using a solar assisted chemically recuperated gas turbine [131].

2.3 Tower Reforming Cycle

Since, as seen with the trough reforming simulations, the reforming process requires a higher operating temperature than the troughs are able to provide, the reformer is now integrated with a solar tower (which can reach higher temperatures as discussed in Chapter 1 [105]) and the tower reformer is then integrated with a combined cycle. This combined cycle integrated with a tower reformer is based on the solar reforming hybrid cycle proposed in [119], however, the analysis here is more in depth in that an optimization of both design and operation is performed for the hybrid cycle, fluctuation of the solar supply is accounted for in both design and operation, and off-design conditions are also considered.

2.3.1 Hybrid Cycle Model Description

The hybrid power cycle flowsheet is shown in Fig. 2-6 and modeled entirely in Aspen Plus®. It is a standard combined cycle with a triple pressure Heat Recovery Steam
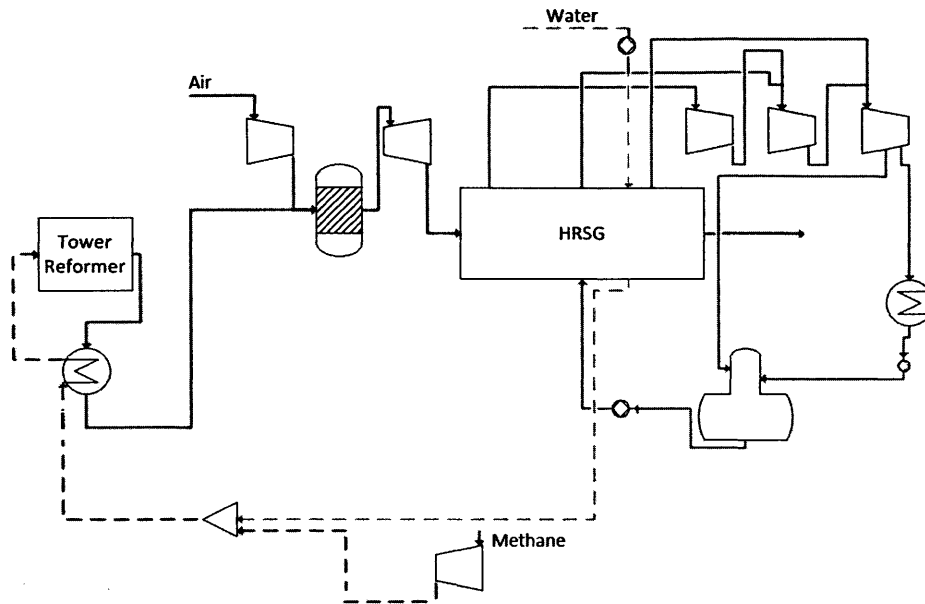
Figure 2-6: Power cycle flowsheet

Generator (HRSG). The solar technology used in this hybrid cycle is a central receiver reformer. The water needed for reforming is first pumped to the pressure of the combustor and then preheated in the HRSG before being mixed with the methane, which is already compressed to the appropriate pressure. The methane and water mixture is then evaporated using the tower reformer outlet in order to turn the water into steam before being sent to the tower reformer. All the syngas created by the reformer is then sent to the gas turbine cycle as the working fluid. The compressed air is sent to the combustor, and the combustion is assumed to be complete and adiabatic. It should be noted that in actual practice, only a portion of the air would be sent to the combustor and then the remaining air would be mixed with the outlet of the combustor for temperature control. However, since the combustor herein is modeled as a black box, thermodynamically both methods will yield the same results. The flue gas is then used in the HRSG of the steam cycle. The steam cycle is designed such that the expanded steam from the high pressure turbine is mixed with the intermediate pressure superheated steam before being sent to the intermediate pressure turbine. The same is also true for the low pressure turbine in that the expanded steam from

65

the intermediate pressure turbine is also mixed with the low pressure steam from the HRSG before being expanded through the low pressure turbine. The outlet of the low pressure steam is split between the deaerator and condenser before being sent back to the HRSG. The pinch values within each section of the HRSG are fixed (discussed in more detail later) and for the compressors and turbines, an isentropic efficiency is utilized to calculate the outlet conditions. The methane is assumed to be an ideal gas and all pressure drops are neglected except for the pressure drop across the HRSG (Section 2.3.2).

For the power cycle model, solar energy is only utilized if there is an input solar share of at least 10%. When there is not enough solar energy, the solar technology is bypassed (i.e., no reforming), and the methane is sent directly to the combustor and no water is needed for reforming. The model is also pseudo steady state and no storage is considered.

Tower Reformer Model

The reformer model is created in Aspen custom modeler and integrates the reformer reactor with the solar receiver. The receiver reactor is assumed to be cylindrical in shape, and the model takes into account optical, radiation, and convection heat losses. The pressure drop across the tower reformer is neglected, and the operating temperature is assumed to be equal to the reforming temperature. An example trend of the variation of the reforming temperature throughout the day is shown in Fig. 2-7. As expected, the more solar energy available (i.e., peak solar energy available at approximately hour 12) the higher the reformer temperature.

The radiation losses are calculated using the following equation [102]:

$$\dot{Q}_{rad} = A\epsilon_{eff}\sigma T^4$$

where A is the area of the receiver, ϵ_{eff} is the effective emissivity of the receiver, and T is the operating temperature of the receiver reactor. The convection heat losses are
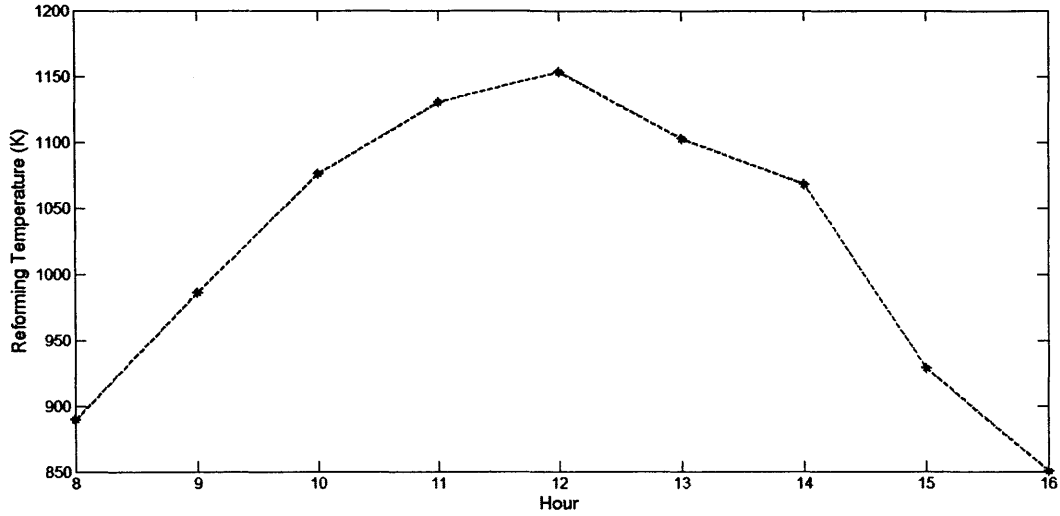
66

Figure 2-7: Reformer Temperature Variation (May 1)

calculated using the following equations [102]:

$$\dot{Q}_{conv} = Ah(T - T_{amb})$$

$$h = 0.557\text{x}10^{-6} \left(\frac{T - T_{amb}}{H}\right)^{0.25} \text{[W/m}^2\text{-K]}$$

where the convection heat transfer coefficient (h) is calculated using the Bejan correlation for vertical chamber with natural convection and H is the height of the receiver. The radiation and convection heat loss variation throughout the day is shown in Figure 2-8. As can be seen from Fig. 2-7 and Fig. 2-8, the higher heat losses correspond to the higher reforming temperatures. However, it should also be noted that heat losses are rather insignificant compared to the heat transfer rate to the receiver with radiation losses accounting for less than 6% of the heat transfer rate to the receiver and the convection losses accounting for less than 1% of the heat transfer rate to the receiver.

The optical efficiency is calculated from the model presented in [79]. This model is used because it gives a time variable optical efficiency, which is more accurate than a time-invariant optical efficiency. This model also uses a biomemtic heliostat pattern
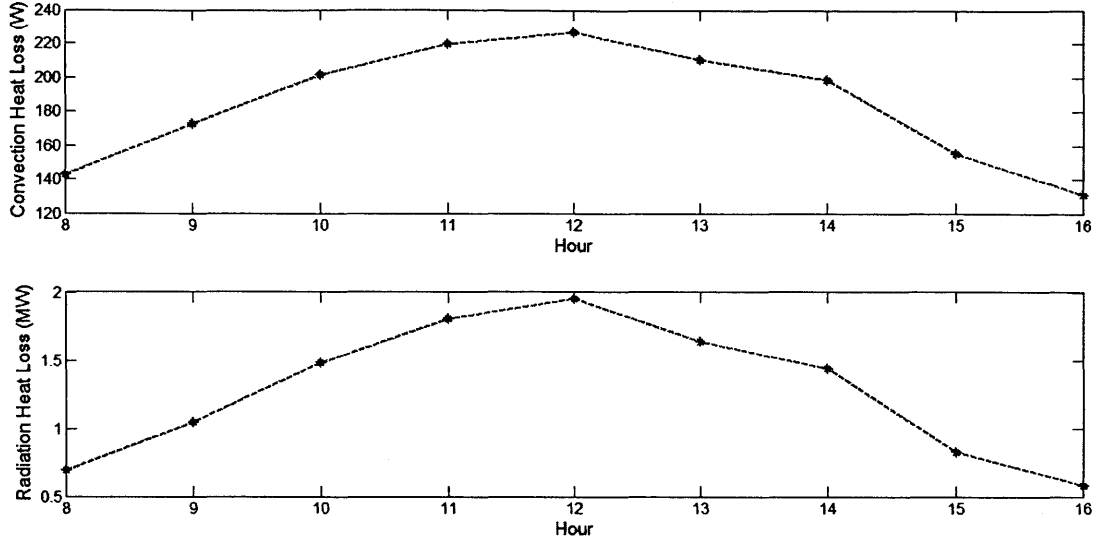
67

Figure 2-8: Convection Heat Loss (Top in W) and Radiation Heat Loss (Bottom in MW) Variation (May 1)

which leads to less land area and higher optical efficiency than traditional heliostat field designs.

The reformer is modeled such that both steam reforming of methane and the water gas shift reaction are taken into account. The possible products are fixed to CH_4, H_2O, H_2, CO_2, and CO, and the reformer model is based on the stoichiometric method for equilibrium. The temperature and outlet composition is calculated using the Law of Mass Action, standard Gibbs free energy of reaction, and an energy balance as shown below:

$$\exp\left(\frac{-\Delta_{R,j}^{o}G(T)}{RT}\right) = \left(\frac{P}{P^o}\right)^{\Delta_{R,j}\nu} \prod_i X_{i,j}^{\nu_{i,j}}$$

$$\eta_{opt}\dot{Q}_{solar} - \dot{Q}_{rad} - \dot{Q}_{conv} = \sum_i \dot{n}_{i,out}\hat{h}_{i,out} - \sum_i \dot{n}_{i,in}\hat{h}_{i,in}$$

where i refers to the specific species, j refers to the specific reaction (stoichiometric), P is the pressure of the reformer, T is the reforming temperature, $\nu_{i,j}$ is the stoichiometric coefficient of species i in reaction j, $X_{i,j}$ is the mole fraction of species i in reaction j, $\Delta_{R,j}^{o}G$ is the Gibbs free energy of reaction at standard pressure of reaction j, η_{opt} is the optical efficiency, $\dot{Q}_{solar}$ is the total solar input (DNI multiplied

68

by heliostat area), $\dot{n}_i$ is the molar flow rate of species i, and $\hat{h}$ (in/out) is the molar enthalpy.

DNI Data

The solar DNI data used in the power cycle model is obtained from the weather station at King Fahd University of Petroleum and Minerals (KFUPM) in Dhaharan, Saudi Arabia. The DNI is given in an hourly interval for an entire year. The DNI data is from the year 2008. Plots of the DNI for the entire day for different times of the year are shown in Fig. 2-9.
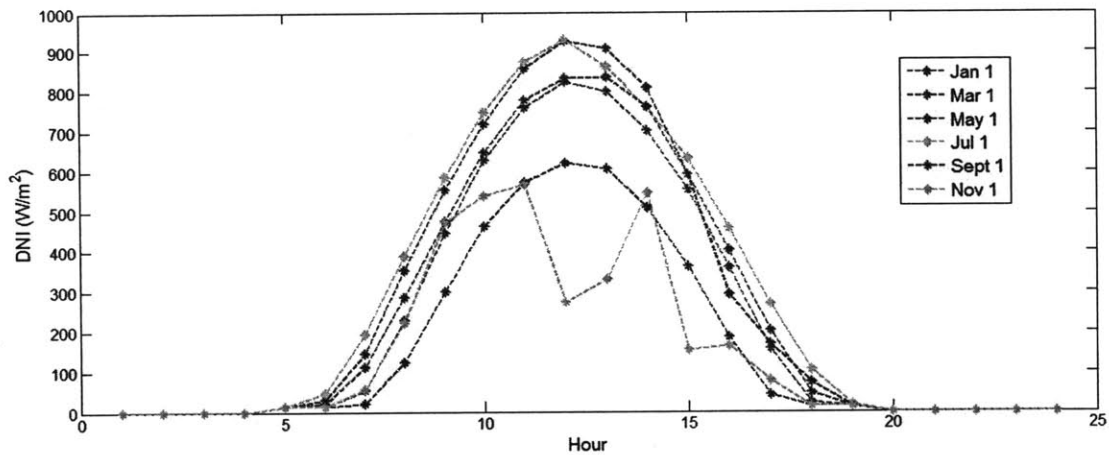
Figure 2-9: DNI trends throughout the day for various days in the year

Note that the DNI is not perfectly symmetric around hour 12 (as you would expect for perfect weather situations). Also, since perfect weather is not assumed, there are anomalies within a day where the DNI values does to follow the expected trend. An example of these anomalies can be seen in Fig. 2-9 with the DNI plot for November 1. On November 1, the DNI value unexpectedly dips at noon rather than reaching a peak indicating cloud coverage or other weather phenomena. In addition to anomalies within a day, there can also be entire days where the solar DNI is much less than ideal. For example, in Fig. 2-10, the DNI values for January 14 are overall significantly lower than both the day before and after it.

69

Figure 2-10: Example of a "cloudy" day: DNI values much less than ideal

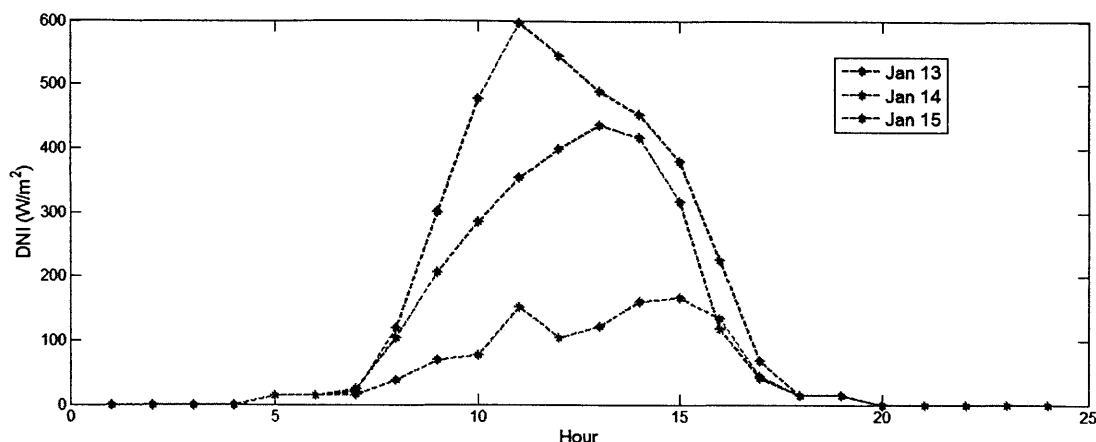Essentially, by not assuming perfect weather, the simulation also captures possible random weather anomalies that would affect whether or not there is enough solar energy available to be used with the hybrid power cycle.

2.3.2 Optimization

After the hybrid cycle model is created, its design and operation is optimized using the built in Aspen Plus® optimizer, which utilizes an SQP method of optimization. The objective function is to maximize the work output for a fixed fuel input and fixed heliostat area (in essence maximizing the first law efficiency) over an entire year (i.e., taking into account fluctuating solar energy supply).

2-Step Optimization Process

Due to the limitations of the Aspen optimizer, the optimization over the entire year is performed using a two step process. The first step is to optimize the cycle over the entire year allowing for both design and operational variables to vary. In reality, only the operational variables would be able to vary throughout the entire year, so this first optimization step, in essence, represents an upper bound on the performance of the cycle (assuming that the global optimum is found). The second step of the optimization process is then to run the optimization again but this time only allowing

70

the operational variables to vary and setting the design variables to a fixed value equal to the average of the different values obtained in step one of the optimization process. In the second step of the optimization process off-design conditions are accounted for, in particular varying isentropic efficiency and pressure drop across the HRSG. To obtain the design volumetric flow rates and enthalpy changes for the isentropic efficiency calculations, the second optimization step is run many times with various design flow rates/enthalpy changes to obtain the best overall performance (i.e., highest overall efficiency).

Isentropic efficiency (2nd Step Only)

The isentropic efficiency for the air compressor, gas turbine, and steam turbines are calculated based on empirical equations shown below.

$$HR = \sqrt{\frac{\Delta H}{\Delta H_{design}}} \qquad VFR = \frac{VF}{VF_{design}}$$

$$\eta_1 = (((A\,HR\,B)\,HR+C)\,HR+D)\,HR+E$$

$$\eta_2 = (((A1\,VFR+B1)\,VFR+C1)\,VFR+D1)\,VFR+E1$$

$$\eta_i = \eta_{opt}\,\eta_1\,\eta_2$$

These equations are a function of the design point enthalpy change across the compressor/turbine (ΔH_{design}), the actual enthalpy change across the compressor/turbine (ΔH), the design volumetric flow rate (VF_{design}), and the actual volumetric flow rate (VF). η_i is the isentropic efficiency of the compresor/turbine. The various constants (A, B, A1, B1, etc.) and the η_{opt} are obtained empirically from manufacturer data [40].

As an example, the efficiency variation of the steam turbines for one day is shown in Fig. 2-11.
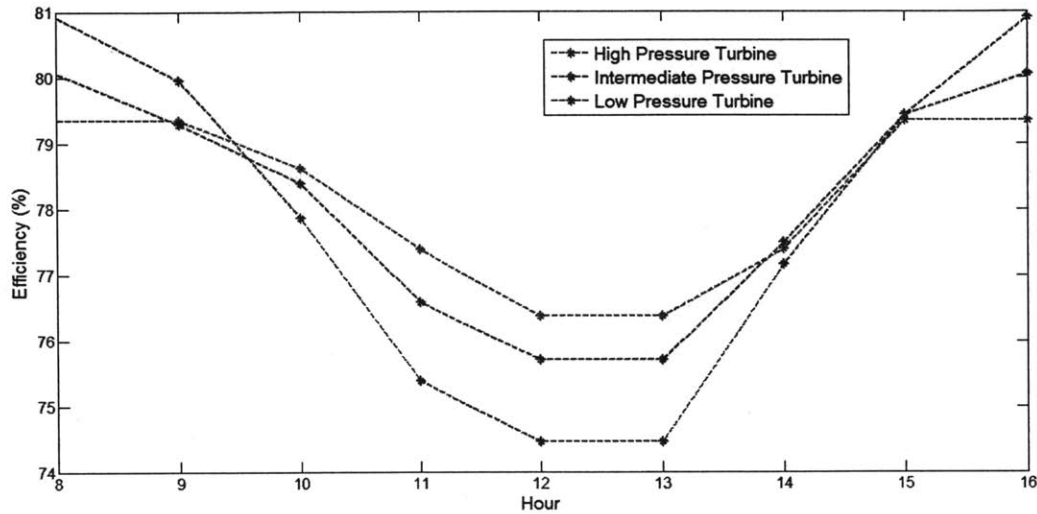
Figure 2-11: Isentropic Efficiency Variation of Steam Turbines for May 1st

HRSG Pressure Drop (2nd Step Only)

The pressure drop is calculated by first calculating the friction factor using the Moody equation shown below:

$$f = .0055 \left(1 + \left(2\text{x}10^4 \frac{\epsilon}{D} + \frac{10^6}{\text{Re}} \right)^{\frac{1}{3}} \right)$$

Then the pressure drop is calculated as follows:

$$\Delta P = f \frac{L}{D} \frac{\rho V^2}{2}$$

Optimization Variables

The optimization (both design and operational) variables and their values/ranges are shown in Tab. 2.5.

As stated previously, the design variables are fixed during the second step of the optimization. The values for these design variables are determined by averaging over the entire year for the values obtained from the first step optimization.

72

Table 2.5: Optimization Variables

Design Variables	Step 1 Range	Step 2 Value
High Pressure [bar]	1-150	81
Intermediate Pressure [bar]	1-150	25
Low Pressure [bar]	1-150	5
High Pressure Superheat Steam Temperature [K]	500-900	850
Intermediate Pressure Superheat Steam Temperature [K]	300-750	700
Operational Variables	**Step 1 Range**	**Step 2 Range**
Low Pressure Steam Flow Rate [kmol/s]	0.001-10	0.001-10
Intermediate Pressure Steam Flow Rate [kmol/s]	0.001-10	0.001-10
High Pressure Steam Flow Rate [kmol/s]	0.001-10	0.001-10
Water (For Reforming) Flow Rate [kmol/s]	0.125-1	0.125-1
Air Flow Rate [kmol/s]	0.01-10	0.01-10
Dearator Flow Rate Fraction	0.01 - 0.99	0.01 - 0.99

Optimization Constraints

The optimization constraints are shown in Tab. 2.6. The first three constraints fix the pinch for each section of the HRSG. The pinch values are based on the ones presented in [95]. It should also be noted that the HRSG area is a fixed parameter. The combustor outlet temperature is fixed by varying the oxygen flow rate. These constraints are implemented within Aspen Plus® as design specifications in order to reduce computation time [128]. Consequently, the optimization problem has no constraints beyond the variable bounds (box-constrained problem).

Table 2.6: Optimization Constraints

Name	Constraint
HPPinch	Pinch Point = 60 K
IPPinch	Pinch Point = 50 K
LPPinch	Pinch Point 10 K
TCOMB	T_{comb}=1600 K

Parameters

There are certain aspects of the cycle that are fixed and not optimized for. These aspects include the HRSG heat exchange areas, the combustor pressure, and condenser temperature. The values used for the parameters are shown in Tab. 2.7.

The fuel flow rate is chosen such that the fuel input is fixed at 100MW. The HRSG area is chosen based on the pinch points for a nominal flow rate. The combustor

Table 2.7: Optimization Parameters

Parameter	Value
Fuel Flow Rate	0.125 kmol/s
Reformer Diameter	5 m
Reformer Height	10 m
Solar Field Area	50,000 m^2
HRSG Area	923 m^2
Combustor Pressure	30 bar
Condenser Temperature	310 K

pressure and condenser temperature are chosen based on typical plant operation [27].
The solar field area is chosen such that the maximum input solar share over the entire
year is 34.4%. Similar to when determining the amount of solar energy for the trough
reforming, the following formula is again used to calculate the required area:

$$X_{s,i} = \frac{\dot{Q}_{solar}}{\dot{Q}_{fuel} + \dot{Q}_{solar}}$$

2.3.3 Optimization Results

Table 2.8: Key Optimization Results

Metric	Value
Annual Cycle Efficiency	47.59%
Annual Incremental Solar Efficiency	26.11%
Maximum Input Solar Share	34.40%
Maximum Output Solar Share	20.52%
Annual Input Solar Share	9.58%
Annual Output Solar Share	5.39%
Annual CO$_2$ Emissions	0.386 kg/kWh

First to summarize the optimization results, Tab. 2.8 shows the values for various
metrics discussed in Chapter 1 [105].All the annual metrics include the time when
there is no solar available. The typical solar share variation throughout the day is
shown in Figure 2-12. It should be noted that only hours during the day in which
the solar is actually used within the hybrid cycle are shown.

As expected, the solar shares - both input and output - follow the trend of the
solar irradiance (i.e., the more solar energy available the higher the input and output
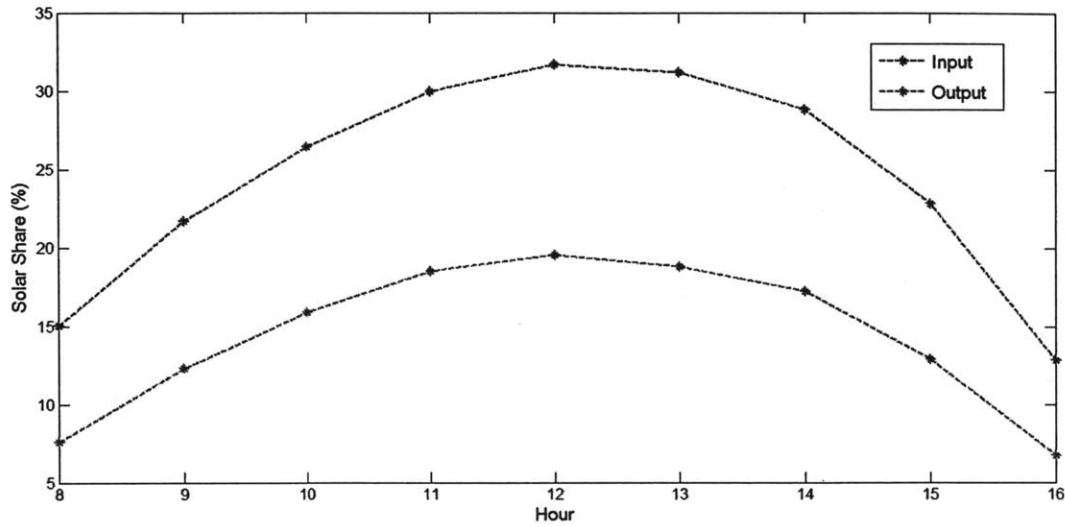
Figure 2-12: Solar Share Throughout Day (May 1)

solar share). As can be seen from Figure 2-12, the magnitude of the output solar share is significantly less than the input solar share, which demonstrates the relative inefficiency of the solar application as compared to the fossil fuel part.

From the optimization, the work output for various days (when solar is available) throughout the year is shown in Fig. 2-13. The work output shown in Fig. 2-13 shows the work for when solar is available and used. The work output trend follows that of the input solar share in that the higher the input solar share, the higher the work output. This trend makes sense because if the input solar share increases, the overall input to the power cycle increases which should lead to a higher output from the cycle.

In addition to the work output of the cycle, the overall cycle efficiency as well as the incremental solar efficiency is investigated. Recall from Chapter 1 [105] that the cycle efficiency and incremental solar efficiency are defined as follows:

$$\eta_I = \frac{\dot{W}}{\dot{Q}_{fuel} + \dot{Q}_{solar}}$$

$$\eta_{net-incr-solar} = \frac{\dot{W} - \eta_{ref}\dot{Q}_{fuel}}{\dot{Q}_{solar}}$$
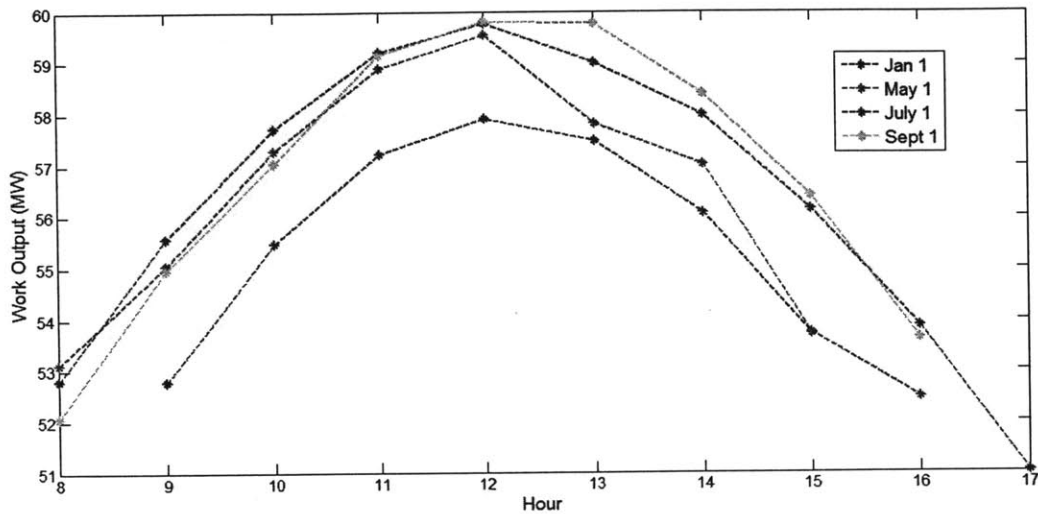
75

Figure 2-13: Work Output Throughout Entire Year

In this analysis, the reference cycle efficiency is obtained by optimizing the cycle flowsheet without the solar reformer. From this optimization the reference cycle efficiency is set at 48.56%. The comparison of these two efficiencies is shown for a particular day in Fig. 2-14.
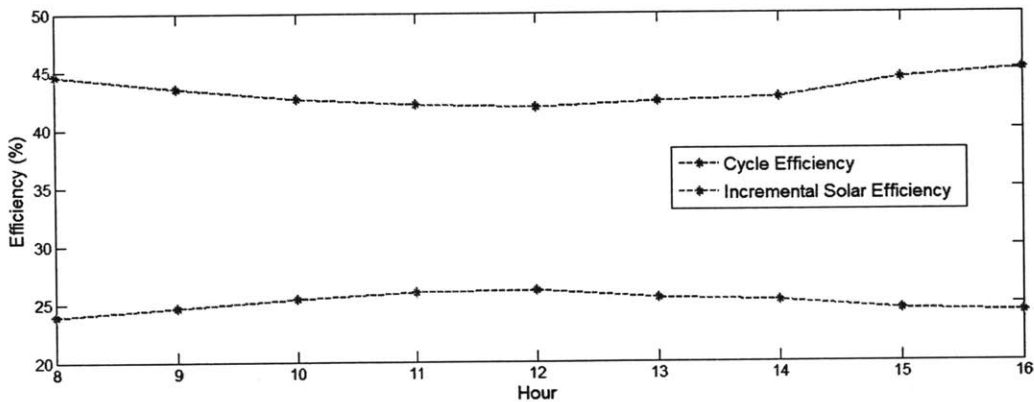

Figure 2-14: Comparison of Cycle and Incremental Solar Efficiency for May 1

For the overall cycle efficiency, it decreases as the input solar share increases. This trend is because the solar part of the hybrid cycle is relatively inefficient when comparing to the fossil fuel part. Therefore, when the solar share is increased, the solar

application has a greater contribution to the overall cycle which means a lower overall cycle efficiency. On the other hand, as can be seen from Fig. 2-14, the incremental solar efficiency has the opposite trend, meaning that the incremental solar efficiency actually increases as the solar share increases. The reason for this trend is because the incremental solar efficiency somewhat represents the efficiency at which the solar energy is utilized within the hybrid cycle. In other words, as the input solar share increases (which corresponds to approaching a peak optical efficiency around noon), the efficiency at which the solar energy is utilized increases, which leads to the trend seen for the incremental solar efficiency.

Another important aspect of this hybrid cycle is the need for flexible fuel combustion. As the reforming temperature is not fixed, the composition of the syngas produced varies throughout the day. Therefore, the combustor must be able to handle fuels with various compositions. Since no storage is considered, during periods of no solar irradiance, the syngas is pure natural gas (assumed to be CH_4 herein). The other extreme composition (observed on May 29, hour 12) is $CH_4 = 0.049$, CO$= 0.123$, and $H_2 = 0.557$, $H_2O= .231$, and $CO_2 = 0.040$ (mole fractions). To illustrate the changing composition within a day, Fig. 2-15 shows the variation in the composition of the syngas throughout a single day. When there is more solar energy available, more reforming occurs and therefore the syngas created contains more hydrogen. It should also be noted that including storage of the reformate will reduce the variation of the fuel entering the combustor.

To compare this solar reforming hybrid cycle to other already existing hybrid technologies a number of different metrics can be used (as discussed in Chapter 1 [105]). The cycle efficiency and solar share are not good measures for comparison because the efficiency for various cycles will automatically be higher but does not take into account the higher cost of certain cycles (i.e., combined cycle versus Rankine cycle) and the solar share is dependent on the solar field size. Therefore, the incremental solar efficiency is used for comparison because it allows for a comparison of not only how efficiently the solar energy is utilized but also a comparison of the relative potential of the various integration methods. The incremental solar efficiency is compared
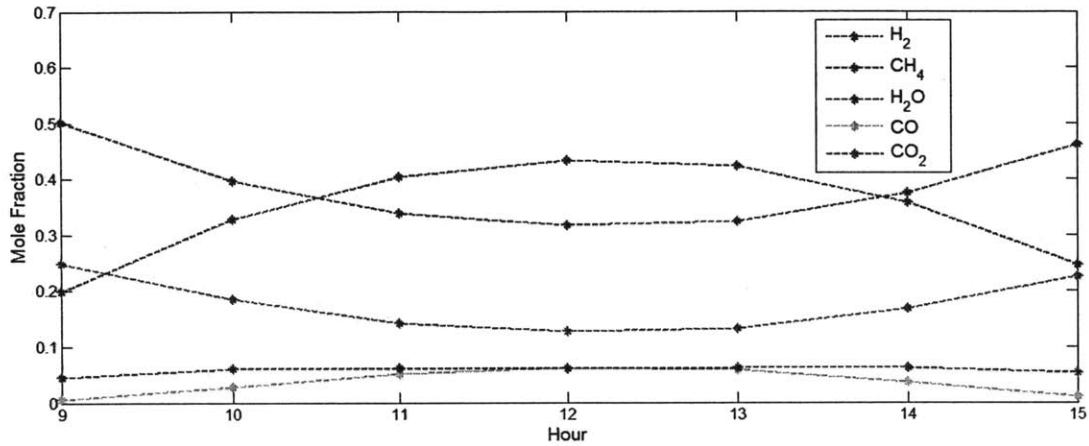
Figure 2-15: Variation in Syngas (Reformate) Composition Throughout Day (Jan 1)

on two different bases: annual and instantaneous. As discussed in Chapter 1 [105], performance metrics should be evaluated on an annual basis as this allows for a more comprehensive view of the performance of the cycle because the solar energy input is variable throughout the year. However, due to the fact that not all previous work report metrics on an annual basis, the instantaneous metric is compared as well.
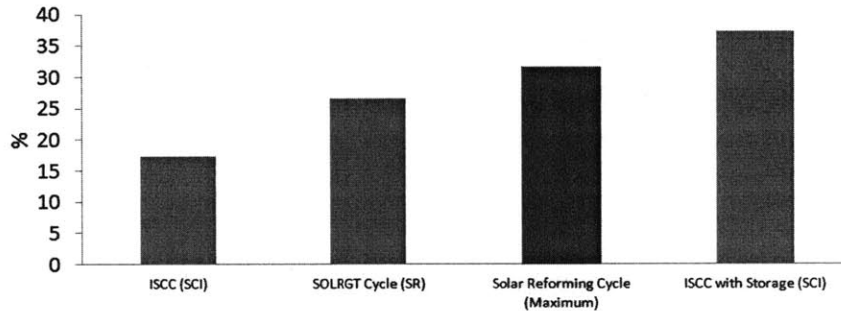
Figure 2-16: Comparison of Instantaneous Incremental Solar Efficiency: SR - Solar Reforming and SCI - Steam Cycle Integration

As can be seen from Fig. 2-16, the instantaneous incremental efficiency is greater than already existing technologies [34, 131] and comparable to a hybrid cycle with storage. This comparison suggests that the solar energy is utilized more efficiently in the solar reforming cycle analyzed here than the other hybrid cycles. It should

78

also be noted that the hybrid cycle under consideration does not take into account storage, but as stated previously, storage is possible by not utilizing all the syngas produced immediately.
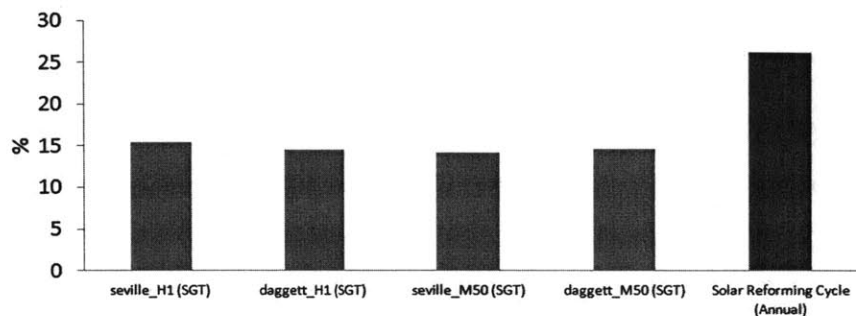

Figure 2-17: Comparison of Annual Incremental Solar Efficiency: SGT - Solarized Gas Turbine

From Fig. 2-17, when comparing on an annual basis with other hybrid technologies [100], the incremental solar efficiency is greater than other existing hybrid technologies, which again suggests that this hybrid solar reforming cycle utilizes the solar energy more efficiently.

Another metric that can be used for comparison to already existing technologies is the linear combination metric proposed in [105]. For this comparison, cycle efficiency and CO_2 emissions are used as the evaluation metrics. Similar to the incremental solar efficiency comparison, both the instantaneous and annual values are used depending on the metrics provided in literature. As can be seen from Fig. 2-18, the plant analyzed (Solar Reforming Cycle) is considered a promising option when compared to the reference plant used for the incremental solar efficiency calculation (solid line); however, when comparing to the state of the art technology such as the GE's Baglan Bay Power Station [2] (dotted line), the plant is considered not viable. While in principle, it is better to compare to the state of the art technology, it should be noted that the combined cycle used for analysis does not contain many of the cycle aspects/components that the state of the art technologies have, such as reheating within the steam cycle and advanced gas turbine technology that utilizes steam from the HRSG [2], that would lead to higher efficiencies. Integrating solar reforming with

79

such a cycle would results in a higher efficiency for the hybrid cycle and demonstrated the full potential of solar reforming. Fig. 2-18 also shows several literature hybrid cycles. While both Seville plants [100] should not be considered, the Daggett plants [100] and the SOLRGT Cycle [131] can be considered promising. Also of note is that the Solar Reforming Cycle (instantaneous) has both a higher cycle efficiency and lower emissions than the SOLRGT cycle (a solar reforming cycle where instantaneous metrics are provided). The Daggett plants have lower emissions than the Solar Reforming Cycle, but lower efficiencies as well, which could lead to higher costs.
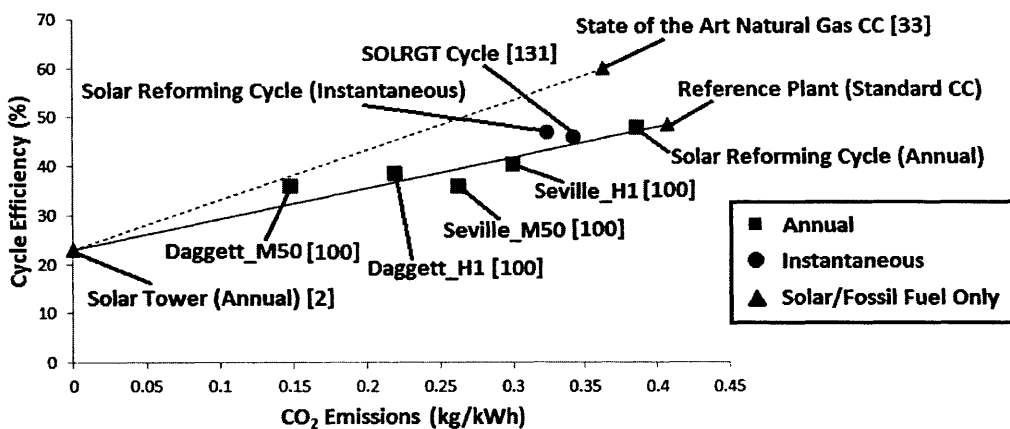
Figure 2-18: Linear Combination Metric Comparison of Analyzed and Literature Hybrid Systems with Solar Only Plant [33], State of the Art Natural Gas CC [2], and Reference Plant

It should be also noted that this linear combination metric is not the same as a positive incremental solar efficiency. To illustrate, consider a fictitious Hybrid Cycle A with a fuel input of 100MW$_t$ and a solar input of 15MW$_t$, and assume that it has an incremental solar efficiency of 21.27% (for the same Reference Plant). The assumed incremental solar efficiency is positive, higher than the literature cycles (annual basis) and similar to the reforming cycle. However, if Hybrid Cycle A was plotted in Fig. 2-18, it would be below the linear combination line which means that a linear combination of solar-only and fossil fuel only plants can have the same overall efficiency and less emissions. In other words, Hybrid Cycle A should not be considered as a viable option despite the relatively high incremental efficiency. In contrast, the

analyzed cycle with reforming is viable.

2.4   Conclusion and Future Work

Overall, reforming as the integration method is a promising method of integration because it can yield high incremental solar efficiencies (even with the inclusion of off-design conditions) and satisfies the linear combination metric for efficiency and emissions. The solar reforming is more suitable to be paired with a solar tower due to the fact that higher operating temperatures are needed in order for any reforming to occur. For the future, the tower reformer model should be refined by obtaining typical residence times and kinetic data. In terms of the optimization, it would be beneficial to simultaneously optimize both design and operational variables rather than use the average design method described previously. In addition, there is a need for flexible combustion which means that the combustor should be able to handle fuels with different compositions. Storage should also be considered in order to limit the variability of the fuel entering the combustor, and also to potentially decrease the amount of fuel consumption. This integration method should also be analyzed with a state of the art combined cycle in order to be able to compare the hybrid cycle to the best available technology and determine true potential. Finally, economic objectives should also be considered in order to determine if the solar reforming cycle has large scale potential.

Bibliography

[1] Abengoa - Abengoa launches first hybrid solar-gas plant in Algeria. http://abengoa.es/corp/web/en/noticias_y_publicaciones/noticias/historico/2011/07_julio/abg_20110714.html, Accessed Nov 18, 2011.

[2] Baglan Bay power station, Cardiff, Wales, UK. http://site.ge-energy.com/about/press/en/articles/baglan_bay_article.pdf, Accessed July 5, 2012.

[3] The California Energy Commission, city of Palmdale Hybrid Power Plant Project. http://www.energy.ca.gov/sitingcases/palmdale/index.html, Accessed Nov 18, 2011.

[4] The Callifornia Energy Commission, victorville 2 Hybrid Power Project. http://www.energy.ca.gov/sitingcases/victorville2/index.html, Accessed Nov 18, 2011.

[5] Florida Power and Light, Martin next generation solar energy center. http://www.fpl.com/environment/solar/martin.shtml, Accessed Nov 18, 2011.

[6] Iran - Yazd integrated solar combined cycle power station. http://www.helioscsp.com/noticia.php?id_not=393, Accessed Nov 22, 2011.

[7] National Renewable Energy Laboratory, Concentrating solar power projects - ISCC Argelia. http://www.nrel.gov/csp/solarpaces/project_detail.cfm/projectID=44, Accessed Nov 22, 2011.

[8] Novatec solars fresnel collector generates superheated steam above 500c. http://www.novatecsolar.com/86-1-Novatec-Solars-Fresnel-collector-generates-superheated-steam-above-500C.html, Accessed April 6, 2012.

[9] Sandia Stirling energy systems set new world record for solar-to-grid conversion efficiency. https://share.sandia.gov, Accessed May 23, 2011.

[10] Solar Millenium, Solar power for Egypt: Flagsol supplied the country's first solar field. http://www.solarmillennium.de/english/technology/references_and_projects/hybrid-power-plant-egypt/kuraymat.html, Accessed Nov 22, 2011.

[11] H. Abdallah and S. Harvey. Thermodynamic analysis of chemically recuperated gas turbines. *International Journal of Thermal Sciences*, 40(4):372–384, 2001.

[12] V. Aga, E. Boschek, and M. Simiano. The value of dispatchability for CSP plants under different market scenarios. In *International SolarPACES Conference, Granada*, 2011.

[13] O. H. Al-Sakaf. Application possibilities of solar thermal power plants in Arab countries. *Renewable Energy*, 14(1-4):1–9, 1998.

[14] H. Alrobaei. Novel integrated gas turbine solar cogeneration power plant. *Desalination*, 220(1-3):574–587, 2008.

[15] A. L. Ávila Marín. Volumetric receivers in solar thermal power plants with central receiver system technology: A review. *Solar Energy*, 85(5):891–910, 2011.

[16] A. Baghernejad and M. Yaghoubi. Exergy analysis of an integrated solar combined cycle system. *Renewable Energy*, 35(10):2157–2164, 2010.

[17] K. Bazex. Mexico - hybrid solar thermal power plant: P066426 - implementation status results report. Technical report, The World Bank, 2011.

[18] M. Becker and M. Böhmer. GAST - The gas-cooled solar tower technology program. Proceedings of the Final Presentation, Lahnstein, Federal Republic of Germany, 1989.

[19] A. Bejan. Unification of 3 different theories concerning the ideal conversion of enclosed radiation. *Journal of Solar Energy Engineering-Transactions of the ASME*, 109(1):46–51, 1987.

[20] A. Bejan. *Advanced Engineering Thermodynamics*. Wiley, 1988.

[21] A. Bejan, G. Tsatsaronis, and M. Moran. *Thermal Design & Optimization*. Wiley and Sons Inc., 1996.

[22] J. Birnbaum, M. Eck, M. Fichtner, T. Hirsch, D. Lehmann, and G. Zimmermann. A direct steam generation solar power plant with integrated thermal storage. *Journal of Solar Energy Engineering-Transactions of the ASME*, 132(3):310–314, 2010.

[23] O. Bolland and H. Undrum. A novel methodology for comparing co2 capture options for natural gas-fired combined cycle plants. *Advances in Environmental Research*, 7(4):901 – 911, 2003.

[24] R. Buck, M. Abele, J. Kunberger, T. Denk, P. Heller, and E. Lupfert. Receiver for solar-hybrid gas turbine and combined cycle systems. *Journal de Physique*, 9(3):537–544, 1999.

[25] R. Buck, T. Brauning, T. Denk, M. Pfänder, P. Schwarzbözl, and F. Tellez. Solar-hybrid gas turbine-based power tower systems (REFOS). *Journal of Solar Energy Engineering-Transactions of the ASME*, 124(1):2–9, 2002.

[26] F. Cavallaro. Multi-criteria decision aid to assess concentrated solar thermal technologies. *Renewable Energy*, 34(7):1678–1685, 2009.

[27] Cleaner Production & Energy Efficiency Center. AZE: Janub 760 MW combined-cycle power plant project. Technical report, Azerenerji Joint Stock Company of the Republic of Azerbaijan for the Asian Development Bank (ADB), 2009.

[28] R. P. Charles, K. W. Davis, and J. L. Smith. Assessment of concentrating solar power technology cost and performance forecasts. Technical report, Sargent & Lundy LLC, 2005.

[29] D. L. Chase. Combined-Cycle development, evolution, and future. Technical report, GE Power Systems, 2000.

[30] C. Y. Chen and C. K. Chen. Power optimization of an endoreversible regenerative Brayton cycle. *Energy*, 21(4):241–247, 1996.

[31] L. Chen, Y. Li, F. Sun, and C. Wu. Power optimization of open-cycle regenerator gas-turbine. *Applied Energy*, 78(2):199–218, 2004.

[32] M. Costea, S. Petrescu, and C. Harman. The effect of irreversibilities on solar Stirling engine cycle performance. *Energy Conversion and Management*, 40(15-16):1723–1731, 1999.

[33] E. A. DeMeo and J. F. Galdo. Renewable energy technology characterizations. Technical report, Electric Power Research Institute (EPRI) and U.S. Department of Energy, 1997.

[34] J. Dersch, M. Geyer, U. Herrmann, S. Jones, B. Kelly, R. Kistner, W. Ortmanns, R. Pitz-Paal, and H. Price. Trough integration into power plants - A study on the performance and economy of integrated solar combined cycle systems. *Energy*, 29(5-6):947–959, 2004.

[35] G. M. Elsaket. Simulating the integrated solar combined cycle for power plants application in Libya. Master's thesis, Cranfield University, UK, 2007.

[36] U. Fisher, C. Sugarmen, A. Ring, and J. Sinai. Gas turbine solarization - Modifications for solar/fuel hybrid operation. *Journal of Solar Energy Engineering-Transactions of the ASME*, 126(3):872–878, 2004.

[37] R. Forristall. Heat transfer analysis and modeling of a parabolic trough solar receiver implemented in engineering equation solver. Technical report, National Renewable Energy Laboratory, 2003.

[38] Y. Gedle, L. Meyer, M. Hoyer, and et al. Exergoeconomic analysis of solar thermal power plants. In *SolarPACES Conference, Granada*, 2011.

[39] A. Ghamarian and A. B. Cambel. Exergy analysis of Illinois no. 6 coal. *Energy*, 7(6):483–488, 1982.

[40] H. Ghasemi and A. Mitsos. Modeling and optimization of a binary geothermal power plant. *Submitted*, 2012.

[41] A. Ghobeity, E. Lizarraga-Garcia, and A. Mitsos. Optimal design and operation of a volumetric solar-thermal energy receiver and storage. Novi Sad, Serbia, July 4-7, 2011. ECOS 2011, The 24th International Conference on Efficiency, Cost, Optimization, Simulation and Environmental Impact of Energy Systems.

[42] A. Ghobeity, C. J. Noone, C. N. Papanicolas, and A. Mitsos. Optimal time-invariant operation of a power and water cogeneration solar-thermal plant. *Solar Energy*, 85(9):2295–2320, June 20, 2011.

[43] A. Ghobeity, C.J. Noone, C.N. Papanicolas, and A. Mitsos. Optimal time-invariant operation of a power and water cogeneration solar-thermal plant. *Solar Energy*, 85(9):2295–2320, 2011.

[44] S. Göktun and H. Yavuz. Thermal efficiency of a regenerative Brayton cycle with isothermal heat addition. *Energy Conversion and Management*, 40(12):1259–1266, 1999.

[45] M. J. Hale. Survey of thermal storage for parabolic trough power plants. Technical report, NREL, 2000.

[46] J. A. Harris and T. G. Lenz. Thermal performance of solar concentrator/cavity receiver systems. *Solar Energy*, 34(2):135–142, 1985.

[47] L. D. Harvey. Solar-hydrogen electricity generation and global CO_2 emission reduction. *International Journal of Hydrogen Energy*, 21(7):583–595, 1996.

[48] P. Heller, M. Pfänder, T. Denk, F. Tellez, A. Valverde, J. Fernandez, and A. Ring. Test and evaluation of a solar powered gas turbine system. *Solar Energy*, 80(10):1225–1230, 2006.

[49] H. Herrmann and D. W. Kearney. Survey of thermal energy storage for parabolic trough power plants. *Journal of Solar Energy Engineering-Transactions of the ASME*, 124(2):145–152, 2002.

[50] D. Hirsch, M. Epstein, and A. Steinfeld. The solar thermal decarbonization of natural gas. *International Journal of Hydrogen Energy*, 26(10):1023–1033, 2001.

[51] D. Hirsch and A. Steinfeld. Solar hydrogen production by thermal decomposition of natural gas using vortex-flow reactor. *International Journal of Hydrogen Energy*, 29(1):47–55, 2004.

[52] H. Hong, H. Jin, J. Ji, Z. Wang, and R. Cai. Solar thermal power cycle with integration of methanol decomposition and middle-temperature solar thermal energy. *Solar Energy*, 78(1):49–58, 2005.

[53] H. Hong, H. Jin, and B. Liu. A novel solar-hybrid gas turbine combined cycle with inherent CO_2 separation using chemical-looping combustion by solar heat source. *Journal of Solar Energy Engineering-Transactions of the ASME*, 128(3):275–284, 2006.

[54] M. Horn, H. Fuhring, and J. Rheinlander. Economic analysis of integrated solar combined cycle power plants: A sample case: The economic feasibility of an ICCS power plant in Egypt. *Energy*, 29(5-6):935–945, 2004.

[55] S. M. Jeter. Maximum conversion efficiency for the utilization of direct solar-radiation. *Solar Energy*, 26(3):231–236, 1981.

[56] E. Kakaras, A. Doukelis, R. Leithner, and N. Aronis. Combined cycle power plant with integrated low temperature heat (LOTHECO). *Applied Thermal Engineering*, 24(11-12):1677–1686, 2004.

[57] S. A. Kalogirou. *Solar Energy Engineering: Processes and Systems*. Elsevier, 2009.

[58] M. Kane, D. Favrat, K. Ziegler, and Y. Allani. Thermoeconomic analysis of advanced solar-fossil combined power plants. *International Journal of Thermodynamics*, 3(4):191–198, 2000.

[59] B. L. Kistler. A user's manual for DELSOL3: A computer code for calculating the optical performance and optimal system design for solar thermal central receiver plants. Technical report, Sandia National Laboratories, 1986.

[60] T. Kodama. High-temperature solar chemistry for converting solar heat to chemical fuels. *Progress in Energy and Combustion Science*, 29(6):567–597, 2003.

[61] T. Kosugi and P. Pak. Economic evaluation of solar thermal hybrid H_2O turbine power generation systems. *Energy*, 28(3):185–198, 2003.

[62] A. Kribus, R. Zaibel, D. Carey, A. Segal, and J. Karni. A solar-driven combined cycle power plant. *Solar Energy*, 62(2):121–129, 1998.

[63] D. Laing, W. D. Steinmann, M. Fib, R. Tamme, T. Brand, and C. Bahl. Solid media thermal storage development and analysis of modular storage operation concepts for parabolic trough power plants. *Journal of Solar Energy Engineering-Transactions of the ASME*, 130(1):011005-1–011005-5, 2008.

[64] E. Y. Lam. A solar-fossil hybrid power system using a combined cycle. *Proc. Int. Solar Energy Soc.*, 2:1151–1155, 1979.

[65] A. Lewandowski and D. Simms. An assessment of linear Fresnel lens concentrators for thermal applications. *Energy*, 12(3-4):333–338, 1987.

[66] D. Li, J. B. Yang, and M. P. Biswal. Quantitative parametric connections between methods for generating noninferior solutions in multiobjective optimization. *European Journal of Operational Research*, 117(1):84–99, 1999.

[67] H. Li, F. Maréchal, and D. Favrat. Evaluation of natural gas combined cycle plants in China through environomic modeling and multi-objective optimization. In *PRES Conference*, 2007.

[68] P. J. Linstrom and W. G. Mallard. NIST Chemistry WebBook, NIST standard reference database number 69. http://webbook.nist.gov, Accessed June 9, 2011.

[69] Maya Livshits and Abraham Kribus. Solar hybrid steam injection gas turbine (stig) cycle. *Solar Energy*, 86(1):190 – 199, 2012.

[70] K. Lovegrove, A. Luzzi, I. Soldiani, and H. Kreetz. Developing ammonia based thermochemical energy storage for dish power plants. *Solar Energy*, 76(1-3):331 – 337, 2004.

[71] N. D. Mancini and A. Mitsos. Conceptual design and analysis of ITM Oxy-combustion power cycles. *Physical Chemistry Chemical Physics*, 13(48):21351–21361, 2011.

[72] J. Mariyappan and D. Anderson. Solar thermal thematic review. Technical report, The Global Environment Facility, 2001.

[73] D. Mills. Advances in solar thermal electricity technology. *Solar Energy*, 76(1-3):19–31, 2004.

[74] D. R. Mills and G. L. Morrison. Compact linear Fresnel reflector solar thermal power plants. *Solar Energy*, 68(3):263–283, 2000.

[75] D. R. Mills, G. L. Morrison, and P. Le Liévre. Project proposal for a compact linear Fresnel reflector solar thermal plant in the Hunter Valley. Technical report, ANZSES Annual Conference - Solar harvest, Newcastle, Australia, 2002.

[76] V. Mirisson, M. Rady, E. Palomo, and E. Arquis. Thermal energy storage systems for electricity production using solar energy direct steam generation technology. *Chemical Engineering and Processing: Process Intensification*, 47(3):499–507, 2008.

[77] M. J. Montes, A. Abánades, J. M. Martínez-Val, and M. Valdés. Solar multiple optimization for a solar-only thermal power plant, using oil as heat transfer fluid in the parabolic trough collectors. *Solar Energy*, 83(12):2165–2176, 2009.

[78] C. J. Noone, A. Ghobeity, A.H. Slocum, G. Tzamtzis, and A. Mitsos. Site selection for hillside central receiver solar thermal plants. *Solar Energy*, 85(5):839–848, 2011.

[79] C. J. Noone, M. Torrilhon, and A. Mitsos. Heliostat field optimization: A new computationally efficient model and biomimetic layout. *Solar Energy*, 86(2):792–803, 2012.

[80] S. Oda and H. Hashem. A case study for three combined cycles of a solar-conventional power generation unit. *Solar & Wind Technology*, 5(3):263–270, 1988.

[81] S. D. Odeh, M. Behnia, and G. L. Morrison. Performance evaluation of solar thermal electric generation systems. *Energy Conversion and Management*, 44(15):2425–2443, 2003.

[82] N. Ozalp, A. Kogan, and M. Epstein. Solar decomposition of fossil fuels as an option for sustainability. *International Journal of Hydrogen Energy*, 34(2):710–720, 2009.

[83] J. E. Pacheco, S. K. Showalter, and W. J. Kolb. Development of molten-salt thermocline thermal storage system for parabolic trough plants. *Journal of Solar Energy Engineering-Transactions of the ASME*, 124(2):153–159, 2002.

[84] P. Pak, T. Hatikawa, and Y. Suzuki. A hybrid power generation system utilizing solar thermal energy with CO_2 recovery based on oxygen combustion method. *Energy Conversion and Management*, 36(6-9):823–826, 1995.

[85] A. Pertsinidis, I. E. Grossmann, and G. J. McRae. Parametric optimization of MILP programs and framework for the parametric optimization of MINLPs. *Computers & Chemical Engineering*, 22(Suppl):S205–S212, 1998.

[86] R. Petela. Exergy of heat radiation. *ASME Journal of Heat Transfer*, 86:187–192, 1964.

[87] R. Petela. Exergy of undiluted thermal radiation. *Solar Energy*, 74(6):469 – 488, 2003.

[88] N. Piatkowski, C. Wieckert, A. W. Weimer, and A. Steinfeld. Solar-driven gasification of carbonaceous feedstock-a review. *Energy & Environmental Science*, 4(1):73–82, 2011.

[89] R. Pitz-Paal, J. Dersch, and B. Milow. European concentrated solar thermal road-mapping. In *Deutsches Zentrum für Luft-und Raumfahrt*, 2004.

[90] W. G. Pollard. The long-range prospects for solar energy: Solar electricity can make only a limited contribution to the nation's large-scale energy needs. *American Scientist*, 64(4):424–429, 1976.

[91] T. Pregger, D. Graf, W. Krewitt, C. Sattler, M. Roeb, and S. Moller. Prospects of solar thermal hydrogen production processes. *International Journal of Hydrogen Energy*, 34(10):4256–4267, 2009.

[92] H. Price, E. Lüpfert, and D. Kearney. Advances in parabolic trough solar power technology. *Journal of Solar Energy Engineering-Transactions of the ASME*, 124(2):109–125, 2002.

[93] H. Price, D. Whitney, and B. Beebe. SMUD Kokhala power tower study. In *Proceedings of the International Solar Energy Conference, San Antonio, TX*, volume 118, pages 273–279, 1996.

[94] B. Prior. Cost and lcoe by generation technology, 2009-2020. http://www.greentechmedia.com/images/wysiwyg/research-blogs/GTM-LCOE-Analysis.pdf, accessed Dec 2011, 2011.

[95] A. Ragland and W. Stenzel. Combined cycle heat recovery optimization. In *Proceedings of International Joint Power Conference, Miami*, 2000.

[96] H. E. Reilly and G. J. Kolb. An evaluation of molten-salt power towers including results of the Solar Two project. Technical report, Sandia National Labs, 2001.

[97] R. Rivero, C. Rendon, and L. Monroy. The exergy of crude oil mixtures and petroleum fractions: Calculation and application. *International Journal of Applied Thermodynamics*, 2(3):115–123, 1999.

[98] M. Romero, R. Buck, and J. Pacheco. An update on solar central receiver systems, projects, and technologies. *Journal of Solar Energy Engineering-Transactions of the ASME*, 124(2):98–108, 2002.

[99] E. Santacana, G. Rackliffe, Le Tang, and Xiaoming Feng. Getting smart. *Power and Energy Magazine, IEEE*, 8:41 –48, March-April 2010.

[100] P. Schwarzbözl, R. Buck, C. Sugarmen, A. Ring, M. Crespo, P. Altwegg, and J. Enrile. Solar gas turbine systems: Design, cost, and perspectives. *Solar Energy*, 80(10):1231–1240, 2006.

[101] A. Segal. WISDOM. In *Proc. Ann. Conf. American Solar Energy Society*, Boulder, CO, USA, 1996. American Solar Energy Society.

[102] A. Segal and M. Epstein. Comparitive performances of tower-top and tower-reflector central solar receivers. *Solar Energy*, 65(4):207–226, 1999.

[103] A. Segal and M. Epstein. Optimized working temperatures of a solar central receiver. *Solar Energy*, 75(6):503–510, 2003.

[104] A. Segal and M. Epstein. Solar ground reformer. *Solar Energy*, 75(6):479–490, 2003.

[105] E. J. Sheu, A. Mitsos, A. A. Eter, E. M. A. Mokheimer, M .A. Habib, and A. Al-Qutub. A review of hybrid solar-fossil fuel power generation systems and performance metrics. *ASME Journal of Solar Energy Engineering*, 134(4):041006:1–17, 2012.

[106] M. Silva, M. Blanco, and V. Ruiz. Integration of solar thermal energy in a conventional power plant: The Colón solar project. *Journal de Physique*, 9(3):189–194, 1999.

[107] A. H. Slocum, J. Buongiorno, C. W. Forsberg, D. S. Codd, and A. T. Paxson. Concentrated solar power system. PCT Patent Application PCT/US10/49474, 2009.

[108] A. H. Slocum, D. S. Codd, J. Buongiorno, C. Forsberg, T. McKrell, J. C. Nave, C. N. Papanicolas, A. Ghobeity, C. J. Noone, S. Passerini, F. Rojas, and A. Mitsos. Concentrated solar power on demand. *Solar Energy*, 85(7):1519–1529, 2011.

[109] D. C. Spanner. *Introduction to thermodynamics*. Experimental Botany. Academic Press, London, New York, second rev. printing edition, 1967.

[110] P. Spath and W. Amos. Assessment of natural gas splitting with a concentrating solar reactor for hydrogen production. Technical report, NREL, 2002.

[111] J. Spelling, M. Russ, B. Laumert, and T. Fransson. A thermoeconomic study of hybrid solar gas-turbine power plants. In *International SolarPACES Conference, Granada*, 2011.

[112] W. Stein, R. Benito, and M. Chensee. Transport and use of solar energy in hydrogen. *Advances in Applied Ceramics*, 106(1-2):2–5, 2007.

[113] A. Steinfeld, M. Brack, A. Meier, A. Weidenkaff, and D. Wuillemin. A solar chemical reactor for co-production of zinc and synthesis gas. *Energy*, 23(10):803–814, 1998.

[114] A. Steinfeld and R. Palumbo. Solar thermochemical process technology. *Encyclopedia of Physical Science & Technology*, 15:237–256, 2001.

[115] M. C. Stoddard, S. E. Faas, C. J. Chiang, and J. A. Dirks. SOLERGY - A computer code for calculating the annual energy from central receiver power plants. Technical report, Sandia National Laboratories, 1987.

[116] M. Sudiro and A. Bertucco. Synthetic fuels by a limited CO_2 emission process which uses both fossil and solar energy. *Energy & Fuels*, 21(6):3668–3675, 2007.

[117] C. Sugarmen, F. Teíllez, R. Buck, J. Medina, P. Altwegg, A. Ring, and et al. SOLGATE: Solar hybrid gas turbine electric power system. Technical report, European Comission, 2002.

[118] S. P. Sukhatme and J. K. Nayak. *Solar Energy: Principles of Thermal Collection and Storage*. McGraw-Hill, 2008.

[119] R. Tamme, R. Buck, M. Epstein, U. Fisher, and C. Sugarmen. Solar upgrading of fuels for generation of electricity. *Journal of Solar Energy Engineering-Transactions of the ASME*, 123(2):160–163, 2001.

[120] M. Thirugnanasambandam, S. Iniyan, and R. Goic. A review of solar thermal technologies. *Renewable and Sustainable Energy Reviews*, 14(1):312–322, 2010.

[121] D. Ugolini, J. Zachary, and J. Park. Options for hybrid solar and conventional fossil plants. Technical report, Bechtel Corporation, 2009.

[122] G. Wall. Exergetics. In *Exergy, Ecology, Democracy, Bucaramanga*, 2009.

[123] L. Wibberley, P. Scaife, and J. Winsen. GHG and cost implications of spinning reserve for high-penetration renewables. Technical report, Australian Cooperative Research Center, 2008.

[124] C. Wu and R. L. Kiang. Power performance of a nonisentropic Brayton cycle. *Journal of Engineering for Gas Turbines and Power*, 113(4):501–504, 1991.

[125] Y. Yang, Y. Cui, H. Hou, X. Guo, Z. Yang, and N. Wang. Research on solar aided coal-fired power generation system and performance analysis. *Science in China Press*, 51(8):1211–1221, 2008.

[126] C. Zamfirescu and I. Dincer. How much exergy can one obtain from incident solar radiation? *Journal of Applied Physics*, 105(4), 2009.

[127] E. Zarza, M. E. Rojas, L. González, J. Caballero, and F. Rueda. INDITEP: The first pre-commercial DSG solar power plant. *Solar Energy*, 80(10):1270–1276, 2006.

[128] H. Zebian, M. Gazzino, and A. Mitsos. Multi-variable optimization of pressurized oxy-coal combustion. *Energy*, 38(1):37 – 57, 2012.

[129] P. Zedtwitz, J. Petrasch, D. Trommer, and A. Steinfeld. Hydrogen production via the solar thermal decarbonization of fossil fuels. *Solar Energy*, 80(10):1333–1337, 2006.

[130] P. Zedtwitz and A. Steinfeld. The solar thermal gasification of coal - Energy conversion efficiency and CO_2 mitigation potential. *Energy*, 28(5):441–456, 2003.

[131] N. Zhang and N. Lior. Use of low/mid-temperature solar heat for thermochemical upgrading of energy, with application to a novel chemically-recuperated gas-turbine power generation (SOLRGT) system. *ASME Conf. Proc.*, 6:313–326, 2009.